NANO · MICRO small
www.small-journal.com

Transducer Systems Integrated into Organ-on-a-Chip Devices: From Detection to Fabrication

*Gabriel M. Ferreira, Patrícia C. Sousa, Susana O. Catarino, and Graça Minas**

Organ-on-a-chip (OoC) devices are an emerging class of advanced microfluidic systems that replicate human physiological functions at the microscale. Enabled by advances in microfabrication techniques (cleanroom-based microfabrication and 3D printing technologies) and tissue engineering, OoCs allow culture cells, manage fluid flow, and recreate biochemical and mechanical stimuli, with high reproducibility and low cost. Therefore, they offer a promising alternative to the traditional preclinical testing of pharmaceutical drugs, contributing to predict the efficacy of new developed drugs. Nevertheless, for this prediction is essential an accurate monitoring of cellular responses over time. However, the effective integration of various types of transducers—optical, electrochemical, mechanical, and resistive—into a single platform for real time monitoring remains a key challenge. This review explores the main transduction techniques used in OoCs, as well as current strategies, limitations, and suggests potential solutions for their integration into functional organ models.

1. Introduction

The Organ-on-a-Chip (OoC) concept is a revolutionary idea that mimics the complex physiological or pathological processes of human tissues and organ models. OoC devices boost the development of drug discovery and screening, and encourage the toxicology research, emulating the behavior of different cells and organs, as the heart, lung, liver, brain, intestine, kidney, blood vessel and lymph node, or even multiple organs.[1–3] OoC development has been promoting the non-use of animals in initial preclinical tests, avoiding ethical and social concerns.[1] In addition, the small size, low cost, fast analysis, energy efficiency, and the ability to establish more realistic physiological models have made OoC devices increasingly more attractive for the advance of biomedical research.[3,4]

The concept of OoC has been emerging for studying drugs, aimed at treating cancer and other diseases, in which the variation of several biological parameters is essential. A key feature of these platforms is their capacity to monitor and control the cellular microenvironment in real time, capturing dynamic changes in biochemical and physical parameters. Critical factors such as temperature, pH, oxygen concentration, glucose, lactate, and mechanical forces influence cell function, differentiation, and response to treatment. These biological requirements define the sensing needs of OoC platforms, shaping both transducer selection and device architecture.

Therefore, the design of an OoC device must be dictated by several important considerations, including transducing mechanisms, materials availability, microfabrication techniques, and finally, the integration of all components and processes into a single platform.[5]

In particular, sensors are essential for the monitorization of biological and physiological parameters. They transform the signal outputted from a physico-bio-chemical quantity (variable to be measured), which usually is in one form of energy into electrical signals, which can be easily processed and interpreted. Optical, chemical, mechanical, and thermal transducers have been the most applied in OoC systems, essentially for sensing pH, oxygen (O_2), glucose, lactate, proteins, pyruvate, temperature, and pressure.[6]

Complementarily, actuators play a key role in regulating and control experimental conditions and dynamic stimuli, helping to replicate physiologically relevant stimuli. They are most commonly used for temperature regulation, fluid mixing, and mechanical stimulation, providing real-time feedback control. These actuators typically operate by converting electrical signals into physical effects, such as localized heating, membrane deformation, or microchannel vibration. Together, sensing and actuation components form closed-loop systems capable of mimicking and dynamically controlling the complex microenvironment of living tissues in vitro. However, one of the critical

G. M. Ferreira, S. O. Catarino, G. Minas
Microelectromechanical Systems Research unit (CMEMS-UMinho)
School of Engineering
Campus de Azurém
University of Minho
Guimarães 4800-058, Portugal
E-mail: gminas@dei.uminho.pt
G. M. Ferreira, P. C. Sousa
International Iberian Nanotechnology Laboratory, INL
Braga 4715-330, Portugal
S. O. Catarino, G. Minas
LABBELS—Associate Laboratory
Braga 4800-122, Portugal

The ORCID identification number(s) for the author(s) of this article can be found under https://doi.org/10.1002/smll.202510425

DOI: 10.1002/smll.202510425

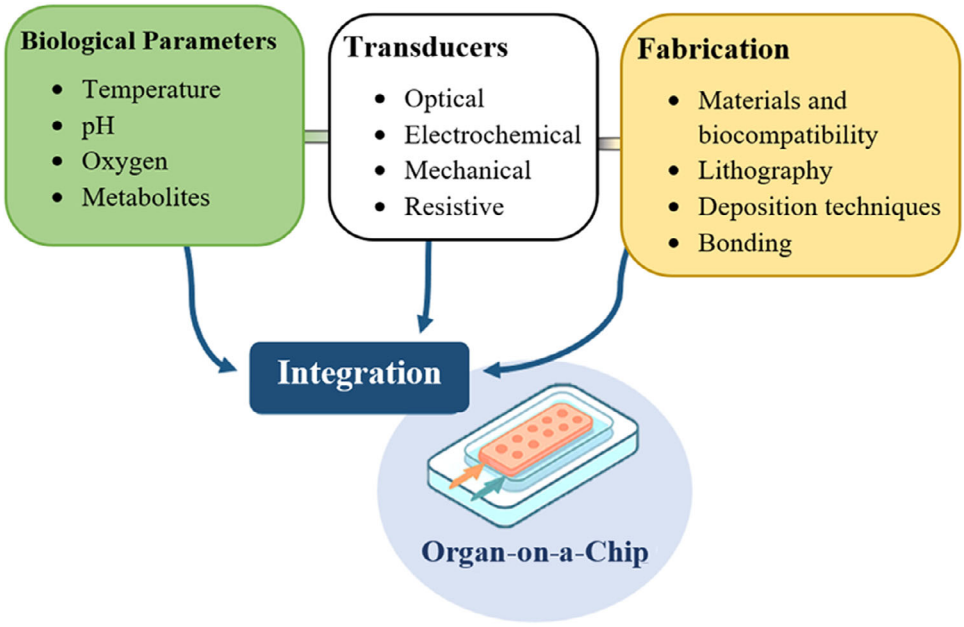

Figure 1. Overview of the multidisciplinary components required for the development of Organ-on-a-Chip platforms, from biological parameters to fabrication and integration.

challenges in the development of clinically relevant OoC devices is the integration of all components, including microfluidic channels/chambers, sensors, biosensors, actuators, and the respective readout and control electronics into a single module. This integration process is essential for continuous, real-time, and multiplexed measurements,[7] and it can influence the sensing elements behavior. Soft lithography, injection moulding, 3D printing, hot embossing, and bonding[8,9] are techniques usually used to fabricate, assemble and/or integrate microfluidic chips. Yet, it is imperative to perform the fabrication and integration in a controlled environment. For instance, optical and electrochemical based-sensors are the most affected by the bonding processes during assembly and integration phases.[10] The adequate assembly method depends on the materials, chip architecture, and fabrication techniques employed.[10] So, although there is no standard method and no recommendation on how to perform the bonding between sensors, the microfluidic chip, and the substrate, there is a plethora of methods reported in the literature that help to draw conclusions regarding the best methods for each specific application.[10]

Since the OoC devices and technologies are becoming a research area with enormous scientific growth and expansion within the last years, it is extremely important to carry out a review focusing on the different types of applied transducers and their integration into OoC systems. Several literature reviews have examined sensors for OoC devices, focusing on detection methods and integration strategies.[4,10–13] However, most of them have not addressed the interplay between sensing and actuation in a unified manner. This review provides a structured and critical analysis of both sensors and actuators designed for integration into OoC systems. It discusses the different physicochemical parameters and biomarkers relevant to monitor and control in OoC systems, the various transduction methods, and their main fabrication techniques, assembly, and integration approaches, along with current strategies, limitations, and potential solutions that are driving significant technological progress. In addition, the review highlights different applications of these transducers, such as in lab-on-a-chip (LoC) systems and in microbioreactors, as foundational technologies for the development of the OoC models. The contribution of this review lies in emphasizing how the integration of sensors and actuators enables more physiologically relevant and real-time responsive organ models. These insights are essential for the adoption of OoC devices as predictive preclinical testing platforms. A schematic representation of the main elements and their interconnection in the development of OoC is shown in **Figure 1**.

2. Relevant Biological Parameters Analysis in OoC

For some in vitro studies, it is important to maintain the culture cells in hypothermia and/or hyperthermia conditions, to cover the optimal cell growth temperatures.[14] Thus, temperature control is essential to minimize differences between the incubator/chamber set point and the in situ temperature, particularly when door opening can affect cell culture.[6] In addition to temperature, pH and O_2 concentration are critical in cell culture. pH can vary significantly in long-term cultures and tissue studies, influence cell differentiation.[14,15] The optimal pH for most cultured cells is ≈7.4, although slight variations are observed among different cell lines.[16,17] While the ideal pH for cell growth varies among cell strains, normal fibroblast lines typically exhibit optimal performance within a pH range between 7.4 and 7.7, whereas transformed cells tend to proliferate more efficiently at a pH between 7.0 and 7.4. Additionally, some studies have indicated that epidermal cells can be maintained at a pH of 5.5.[16] However, certain pathological conditions can alter the pH of cells and their surrounding media during proliferation. For instance, as a cell undergoes tumorigenic transformation, the

extracellular environment experiences a pH reduction from 7.4 to ≈6.5–7.0, while the intracellular pH becomes more acidic, to values between 4.5 and 5.5.[18] Small fluctuations in cellular pH, typically within 0.1–0.6 units, naturally occur as part of normal cell activity and metabolism.[19] These variations reflect changes in ion transport and energy balance that regulate many biological processes, such as growth, signalling, and protein synthesis.[19] Although subtle, they are essential indicators of cell health and function. Therefore, accurate in situ pH monitoring is thus crucial for assessing cell health and drug efficacy.[20,15]

Another relevant parameter is oxygen. It is one of the main components of cellular respiration and energy production, being crucial in cell metabolism and function.[21] It presents differentiated values in cancer and healthy cells/tissues. Therefore, an accurate monitoring and control of this parameter is essential in OoC system.[22] For instance, typical oxygen tensions range from 90–110 mmHg (12–14% O_2) in brain tissue, 27–49 mmHg (3.6-6.4% O_2) in bone marrow, and 30–90 mmHg (3.9–12% O_2) in liver tissue. These variations in oxygen concentration are not only tissue-specific but also directly influence cellular enzymatic activity.[23] Several intracellular enzymes, are oxygen-dependent in the range of 30–200 µM O_2, indicating that even small fluctuations in oxygen levels can alter metabolic and transcriptional pathways.[23] Consequently, sensors designed for OoC platforms must provide high sensitivity and resolution, capable of detecting oxygen changes below 10 µM to accurately mimic physiological and pathological oxygen dynamics. In addition to oxygen, other environmental parameters, such as pressure and humidity, and also biochemical analytes (proteins, glucose, and lactase) need to be analysed, depending on the intended OoC function.[14,24,25] Glucose and lactate monitoring is crucial to treat diabetic patients, assess cellular metabolism, and maintain physiological homeostasis.[26,27] Glucose concentrations typically range between 2 and 6 g L^{-1} (≈11–33 mM), requiring sensors with wide dynamic range, high resolution (≈0.1–0.5 mM), and fast response times,[28,29] Lactate, produced through glycolysis even under normoxic conditions, accumulates extracellularly, reducing pH and indicating altered metabolic states.[30] Thus, both analytes are essential biomarkers for evaluating tissue function and disease progression in OoC platforms.

Understanding and controlling these biological, physical, and chemical parameters is fundamental to guarantee physiologically relevant microenvironments required for viable OoC systems and for seeking the efficacy of a drug therapy. Therefore, the integration of in situ transducers, in the OoC cellular model and/or in the microfluidics network, which convert those variables into measurable electrical signals is of utmost importance for effectively multi-parametric real-time monitoring. This translation is achieved through different transduction mechanisms, which bridge the biological and the electronic readout domains.

3. Transducers

3.1. Optical Transducers

Optical detection is widely employed in OoCs mainly due to its real-time monitoring capability, flexibility, high sensitivity, compact size, immunity to electromagnetic interference, and less dependence to pH and temperature changes. As schematized in **Figure 2**, it is employed when the materials or samples under analysis, either alone or in combination with a specific dye, exhibit characteristic optical properties, particularly in terms of absorption, luminescence, fluorescence, reflectance, or refractive index.[11,24,31] For its proper implementation, excellent transparent materials are required in the OoC platform, assuring a better transmission of the optical signals. Typically, those materials are PDMS, glass, and PMMA, enabling also a fast and easy OoC integration.[11] Furthermore, optical transducers allow for a remote and non-invasive detection, which advantages long-term measurements. In most of the optical methods, the light that targets the sample is subsequently directed to an optical transducer for their electric conversion and quantification. Optical sensors have been widely used and implemented in OoC, mainly for pH, oxygen, glucose, and lactate, as summarized in **Table 1**.

3.1.1. pH Detection

Optical methods have been reported in literature for pH sensing, mostly based in absorbance and luminescence approaches.[31] As presented by Wu et al.[32] and Khalid et al.,[33] pH can be monitored in micro-scale cell culture environments for liver and heart-on-a-chip applications, by measuring the optical properties of phenol red, normally contained in culture medium.[32–34] The phenol red is a non-toxic, non-invasive, colorimetric pH indicator widely used in cell culture, particularly due to its ability to visual output a change in its color, from yellow to bright pink, when the pH of the culture medium changes from acid to alkaline, bellow 6.2 and above pH 8.2, respectively, with an optical absorbance peak at 560 nm.[35,36] In particular, Wu et al.[32] used a light emitting diode (LED) at 568 nm wavelength, one optical fiber to connect the sample to the light source and another one to connect the sample to a photodiode used as the optical sensor. In this setup, the light passes through a polydimethylsiloxane (PDMS) microfluidic chip, then passes through the sample solution and through a thin glass cover slide, finally reaching the photodiode. The phenol red dye was also used by Khalid et al. for pH measurements. The detection was performed using a white LED, an optical filter and a photodiode. Khalid et al.[33] achieved a sensitivity of 0.489 V pH^{-1}, while Wu et al.[32] achieved a 0.83 V pH^{-1} sensitivity. Also, Shaegh et al.[37] and Zhang et al.[38] quantified pH using phenol red and a silicon (Si) photodiode for readout, with a sensitivity close to 0.160 V pH^{-1} for both systems. These systems comprised a white LED, an optical filter (at 515 nm) and a photodiode. Based on a miniaturized system, Santos et al.[39] explored the optical properties of the EGM-2 *Endothelial Cell Growth Medium-2 BulletKit* at different pH values, also employing the phenol red as the pH indicator (already included in the culture medium), to develop an optical sensor able for pH detection of the culture medium flowing in the OoC microfluidic chamber.[39] The authors proposed a microsystem, based on CMOS photodiodes and current-to-frequency converters (**Figure 3A**), to mitigate the problems found in recent methods, which involve complex and non-miniaturized systems with commercial photodiodes,[38] optical fibers,[40] sol–gel filters,[41] and optical microresonators.[42] The microsystem was fabricated through the UMC L180 MM/RF CMOS technology, and on top a PDMS microchannel/microchamber was bonded. By evaluating the slopes

Table 1. Comparison of optical methods and transducers toward integration in LoC/OoC platforms.

Refs.	Parameter	Detection Method /dye or biomarker	Transducer	Sensitivity	LOD	Applications
[32]	pH	Absorbance / Phenol Red	Commercial photodiode	0.83 V pH^{-1} (6.8–7.8)	0.2 pH	Cell culture
[38]	pH	Absorbance / Phenol Red	Si photodiode	0.159 V pH^{-1}	NR	Liver-and-heart-on a-chip
[33,34]	pH	Absorbance / Phenol Red	Commercial photodiode	0.489 V pH^{-1}	NR	Lung cancer-on-a-chip Liver-on-a-chip
[39]	pH	Absorbance / Phenol Red	CMOS photodiode from UMC 0.18 µm + IF Converter	1 kHz pH^{-1}	4.4–7.7 pH (0.1 pH of resolution)	Culture medium in an organ on a chip device
[46]	pH	Astigmatism / PSL layer	CCD sensor	54–94 pixel pH^{-1}	NR	Single-cell behavior and evaluating the effectiveness of drugs
[37]	pH	Absorbance / Phenol Red	Si photodiode	160 ± 3 mV pH^{-1}	NR	Microfluidic cell culture and organ-on-a-chip device
[44]	pH	Absorbance / Phenol Red	Commercial photoresistor	66 ± 2 mV pH^{-1}	NR	Mimic drug-induced lung injury
[45]	pH	Luminescence / OHC12	NR	NR	0.003 pH	Mammalian cells
[64]	pH	Ratiometric Fluorescence / FITC	NR	0.2432 AU/pH	5–8 pH	Tumor models and drug screening
[50,51]	O_2	Luminescence / PtTPTBPF	NR	NR	0.009 hPa	Online monitoring of enzyme transformations
[37]	O_2	Luminescence / Ru(dpp)	NR	6 mV/[%O2]	NR	Microfluidic cell culture and organ-on-a-chip device
[47]	O_2	Fluorescence / PtTFPP	NR	NR	NR	Cell culture
[38]	O_2	Fluorescence / Ru(dpp)	Si photodiode	7 mV/O_2%	NR	liver-and-heart-on a- chip
[49]	O_2	Fluorescence / PtOEP	NR	NR	0–9 ppm	Liver-on-a-chip
[52]	O_2	Luminescence / PtOEPK	Si photodiode	NR	120 ppb	Tissue engineering, cell culturing, and miniaturized bio-assay
[48]	O_2	Luminescence / PtTFPP	NR	NR	NR	Cellular response
[53]	O_2	Luminescence / $[Ru(dpp)^3]^{2+}$	Photodiode of TSMC 0.18 µm-CMOS process	NR	NR	Cell culture
[26]	Glucose	Absorbance / GOD	Commercial light to voltage converter	27.2 µU dl s^{-1} mg^{-1}	25–300 mg dl^{-1}	Clinical diagnosis
[27]	Glucose	Luminescence / GOD	CCD sensor	NR	0.37–4 mM	Cell culture
[56]	Glucose	Transmission NIR spectroscopy	Commercial photodiodes	NR	1–70 mM	Human serum
[61]	Glucose	Diffuse reflectance NIR spectroscopy	InGaAs photodiode array	NR	50–500 mg dl−1	Forearm skin
[30]	Lactate	Fluorescence optical fiber / NADH	NR	NR	0.06–1 mM	Tumor progression
[63]	Endothelial growth factor	Fluorescence/Protein	CMOS photodiode	NR	NR	Cellular response

NR- Not reported

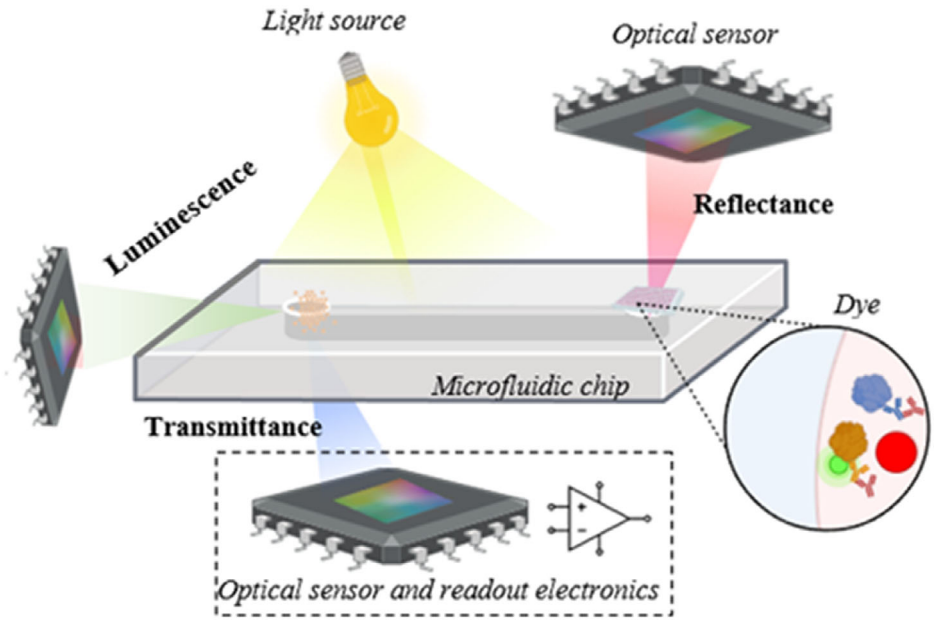

Figure 2. Schematic of different optical detection techniques in a microfluidic chip. The light source illuminates the sample inside the chip, where an indicator dye interacts with the target analytes. The transmitted, reflected or luminescented light is captured by an optical sensor, enabling the analysis of the sample optical properties, such as transmittance, reflectance, luminescence, and refractive index. The readout signals are electronically processed to obtain the data.

between the transmittance values at three specific wavelengths (500, 560, and 600 nm), the microsystem was able to distinguish pH values from 7.7 to 4.4, with a resolution of 0.1 pH units. These slopes' methodology overcome the limitation referred by some authors that the optical detection of pH by phenol red has a limited pH range, typically around pH 6.8 to 8.4.[43] While some authors use only one of the following wavelengths, 515,[37] 560,[44] or 568 nm,[32] Santos et al. used three wavelengths (500, 560, and 600 nm), achieving greater accuracy in determining the absorbance of phenol red.[39] Another optical method for pH detection in a microfluidic system with cell media was described by Müller et al.,[45] using the luminescence of OHC12 dye, as presented in Figure 3B.[45] The pH indicator was excited with red light (620 nm), and their emitted light was in the Near-Infrared (NIR) range. Optical fibers were used to guide the light to an optic block. The sensor presented a resolution of 0.003 pH units with a response time of ≈30 s for a pH shift of 0.5 pH units, from pH 7 to 7.5.[45] Despite the better resolution, this detection method is more complex when a complete integration in a single module is needed. Also, the long-term monitoring can be compromised due to the sensor spot reusability.

Besides absorbance and luminescence, a new optical method was used by Moghaddam et al.,[46] called astigmatism method. It is based on the use of the swelling and shrinkage of chitosan-tetraethyl-orthosilicate-PDMS as a pH-sensitive layer (PSL). The authors used a setup comprising two cylindrical lenses with perpendicular axes and an objective lens, as well as a 667 nm wavelength LED to illuminate the sample. The working principle of the sensor is based on the swelling of the PSL layer when exposed to different pH values. Therefore, by measuring the PSL volume changes, the pH of passing buffers can be identified. At the same time, the divergence of the light reflected from the PSL surface changes by alternating the distance between the objective lens and the surface. After the reflected light passes through two cylindrical lenses, the shape of the beam appears on a 5 MP charge-coupled device (CCD). The method achieved a sensitivity of 54–94 pixels pH^{-1}.[46]

When comparing the different optical pH sensing strategies, absorbance-based methods stand out for their higher usability, simplicity, low cost, low power consumption, and ease of integration, as they can directly use phenol red present in most culture media. However, phenol red may feature a limited pH range (typically 6.8–8.4) not covering all physiological changes, and the absorbance readings can be influenced by medium composition and optical alignment, which requires careful calibration and control. Luminescence-based sensors, on the other hand, offer higher resolution and lower detection limits, making them suitable for monitoring subtle pH variations. However, their integration can be more complex, requiring additional excitation sources, optical filtering, and an even more accurate optical alignment. More advanced techniques, such as astigmatism-based sensing, allow label-free and highly sensitive measurements, but involve bulky and less practical optical setups that are not yet optimized for compact OoC platforms. Overall, while absorbance remains the most practical option for rapid prototyping and integration, luminescent sensors are more promising for high performance.

3.1.2. Oxygen Detection

Oxygen detection in OoC platforms relies predominantly on luminescence-based methods due to their high sensitivity and suitability for continuous, non-invasive monitoring. It

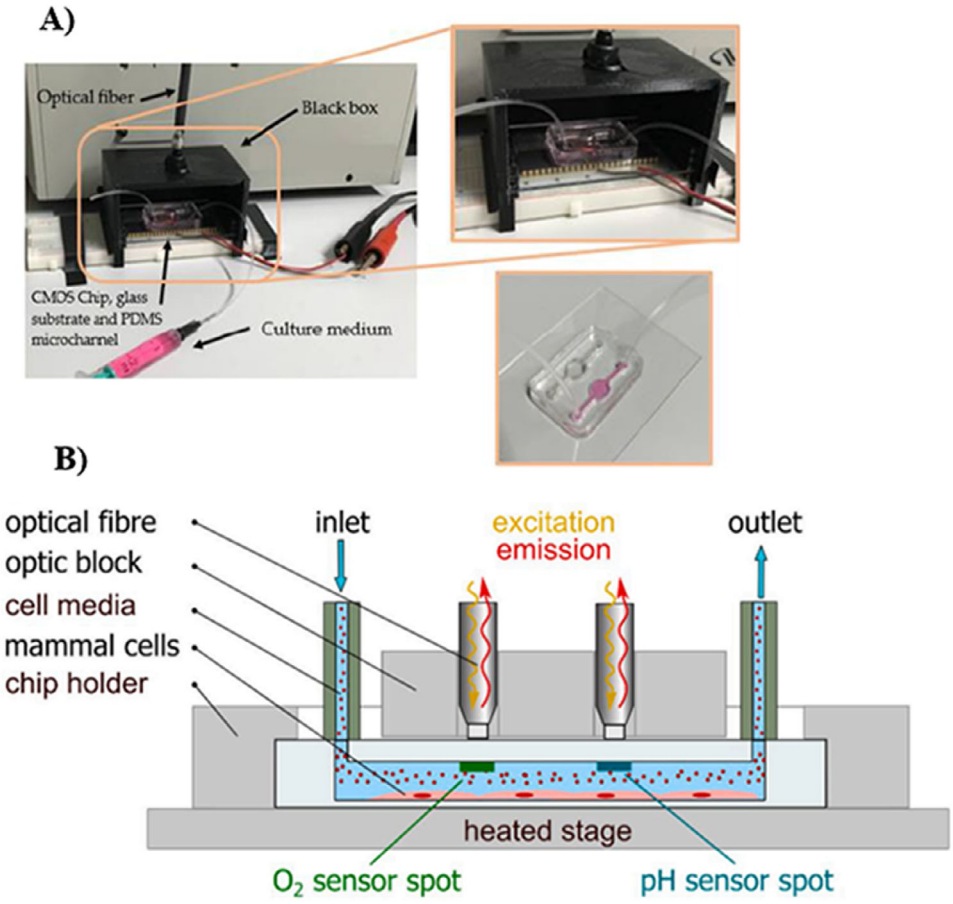

Figure 3. A) Setup for the transmittance measurements of the culture medium at different pH levels, presented by Santos et al.[39] Reproduced from[39] with permission from MDPI, under a Creative Commons Attribution (CC BY) license. Copyright 2024, MDPI. B) Concept of the microfluidic chip utilized by Müller et al.[45] Reproduced from[45] with permission from Elsevier, under a Creative Commons Attribution (CC BY) license. Copyright 2021, Elsevier.

uses either fluorescence or phosphorescence dyes that respond to O_2 molecules as a quencher available inside the chip.[21] Few examples of the most used dyes are: Platinum (II) tetrakis(pentafluorophenyl)porphyrin (PtTFPP),[47,48] Platinium (II) octaethylporphyrin (PtOEP),[49] Platinum (II)-meso-tetra(4-fluorophenyl)tetrabenzoporphyrin (PtTPTBPF),[50,51] Ruthenium-tris(4,7-diphenyl-1,10-phenanthroline) dichloride (Ru(dpp)),[37,38] and Singlet O_2 sensor green (SOSG).

Muller et.al.[45] integrated the previous described pH luminescence sensor with a O_2 sensor (Figure 2B), taking the luminescence optical properties of polymer particles stained with oxygen sensitive PtTPTBPF.[45] These particles are excited with red light (620 nm) and emit in the NIR range of the electromagnetic spectrum, like the used pH indicator, which simplifies the light source and detection setup. The lifetime of the excited dye molecule is proportional to the oxygen partial pressure and is used as a robust, intensity independent parameter.[42]

The sensors designed by Shaegh et al.[37] and Zhang et al.[38] consist of $[Ru(dpp)_3]^{2+}Cl_2$–tris(4,7-diphenyl-1,10- phenanthroline)ruthenium (II) chloride as an oxygen indicator, with an excitation wavelength at 463 nm and a maximum emission at 618 nm. The designed sensors presented a sensitivity of 6 mV/[%O_2][37] and 7 mV/[%O_2],[38] respectively. Shaegh et al.[37] used a Si photodiode to receive the light emitted by the oxygen indicator. Another option, presented by Matsumoto et al.,[49] is the use of a polystyrene (PS) layer containing PtOEP, with an excitation wavelength at 510–560 nm and a fluorescence emission wavelength at 650 nm. Matsumoto et al.[49] achieved a detection range of 0–9 ppm, detecting ultralow oxygen levels. Furthermore, Vollmer et al.[52] selected Pt octaethyl-porphyrin-ketone (PtOEPK) as the O_2 dye due to its desirable optical properties and compatibility with readily available and inexpensive solid-state electronic components. Its excitation and emission wavelengths are at 590 and 760 nm, respectively. A LED, centred at a 590 nm wavelength, was positioned vertically directly above a Si photodiode.[47] The system presented a limit of detection (LOD) of 120 ppb.

Furthermore, some authors used CMOS technology for optical detection of fluorescent light, taking advantage of low dimensions and high integration density.[53,54] Daivasagaya et al.[53] studied and described a compact luminescent gaseous O_2 sensor microsystem, using CMOS technology from TSMC 0.18 µm-CMOS process. The microsystem is composed by an array of 32 × 32 photodetectors (1024 elements) as active pixel sensors, and each pixel includes a high-gain p-n-p phototransistor to convert the detected optical signals into electrical currents

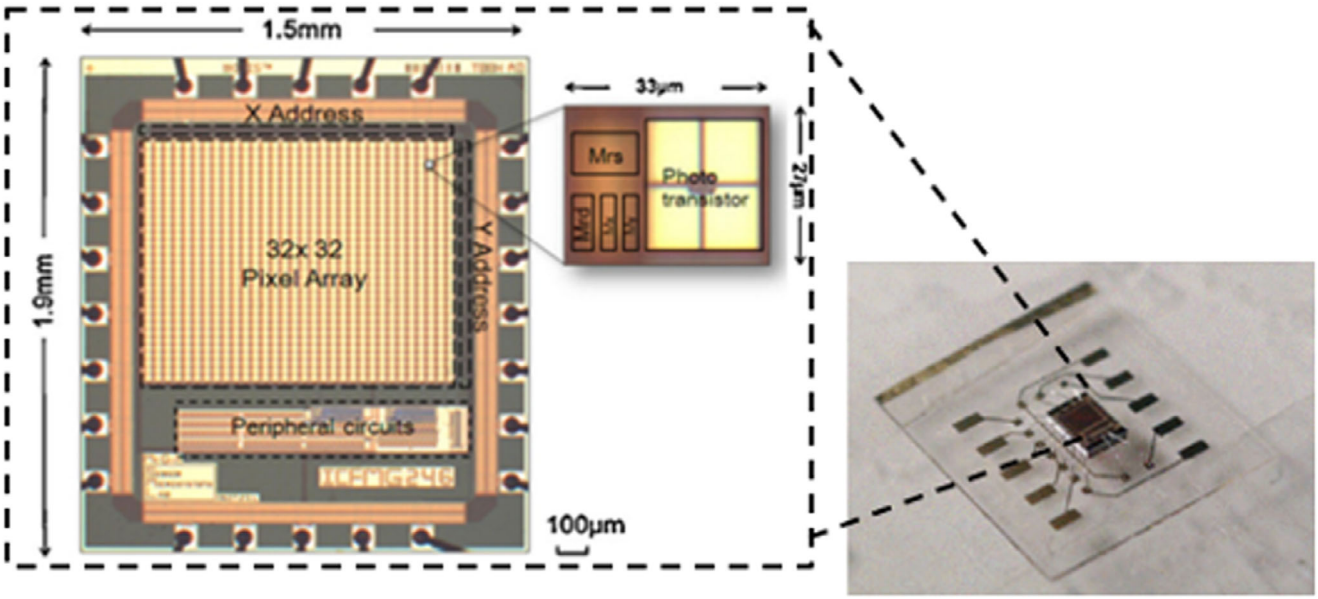

Figure 4. A Microphotograph of the CMOS imager IC. The inset picture shows a single active pixel sensor. Complete packaged imager IC, developed by Daivasagaya et al.[53] Reproduced from[53] with permission from Elsevier. Copyright 2011, Elsevier.

(**Figure 4**). For each readout pixel, the authors designed a correlated doubling sampling circuit and an integrator circuit. It was used a 470 nm LED as excitation source, and a tris(4,7-diphenyl-1,10-phenanthroline) ruthenium. (II) ($[Ru(dpp)_3]^{2+}$) dye. The considered dye emits light at 600 nm.[53]

Taken together, these studies highlight the diversity of luminescent indicators and strategies available for oxygen sensing in OoC systems. While ruthenium-based indicators are commonly used due to their accessibility and ease of integration, platinum-based dyes are often selected for applications requiring higher sensitivity and long-term stability. The choice of the detection architecture, whether intensity or lifetime-based, also strongly influences the performance, cost, and integration complexity of the final platform.

3.1.3. Glucose, Lactate, and Other Analytes Monitoring

In the literature, several methods have been reported to detect glucose optically, including absorbance,[26] luminescence,[27,55] NIR spectroscopy[56] and photoacoustics.[57,58] Currently, photoacoustic is mostly used for measurements directly on skin, and is being a target method due to the raising interest in non-invasive glucose sensors. Its miniaturization for LoC and/or OoC is a promising area of research, which could lead to advances in human tissue models and more accurate detection systems.[59]

Srinivasan et al.[26] presented an optical glucose sensor with an electrowetting chip fitted for fluidic operations and chemical processes, also including a non-invasive optical absorbance measurement system. For detection, the described setup consists of a green LED with emission at 545 nm, a photodiode, and an amplifier integrated on the same device for light to voltage conversion (**Figure 5A**). The device presented a sensitivity of 27.2 µAU dl s^{-1} mg^{-1} (AU stands for absorbance units) and a 25–300 mg dl^{-1} LOD. On the other hand, Park et al.[27] developed an optical glucose sensor film, fabricated by a simple process, by using commercial pressure sensitive paint with an emission light at 655 nm. The sensor is based on the optical detection of the oxygen consumed by the glucose oxidase (GOD)-catalysed oxidation of β-D-Glucose (Figure 5B). The methodology for the measurements included an excitation light source at 420 nm, a CCD camera, optical filters, and a spectrometer.[27] The sensor presented a LOD of 0.37 mM. However, as the concentration of GOD increased, the LOD value became smaller, and the linear detection range also tended to be reduced.[27]

Near-infrared (NIR) spectroscopy offers two fundamental measurement modes for glucose detection:[58] transmittance,[58,60] and reflectance.[61] Ryckeboer et al.[56,58] demonstrated how the transmission spectra of aqueous glucose solutions change due to the presence of glucose. The transmission was measured for different glucose solutions using a fiber array, an optical chip composed of a Si waveguide, a LED with emission centred at 1570 nm, and a tunable optical filter, for the 1540–1610 nm range. The setup presented a glucose detection range of 1–36 mM and a resolution of 1.14 mM.[56,58] Based on the same measurement method, Goodarzi et al.[60] achieved an accuracy of 0.56 mM within a detection range of 1–30 mM.[60]On the other hand, Maruo et al.[61] presented a NIR-based sensor using diffuse reflectance detection, obtaining a glucose detection range of 50–500 mg dl^{-1}, with an accuracy of 27.2 mg dl^{-1}.[61] Both arrangements used non-miniaturized systems, composed by commercial photodiodes, LEDs, and optical fibers.

Lactate concentration detection is also a key parameter for studying the metabolic alterations in tumor progression. However, the number of optical lactate sensors validated for use in cell cultures is limited due to challenges such as biocompatibility, selectivity, and interference from the culture medium.[62] However, Zheng et al.[30] described an optical fiber nanosensor

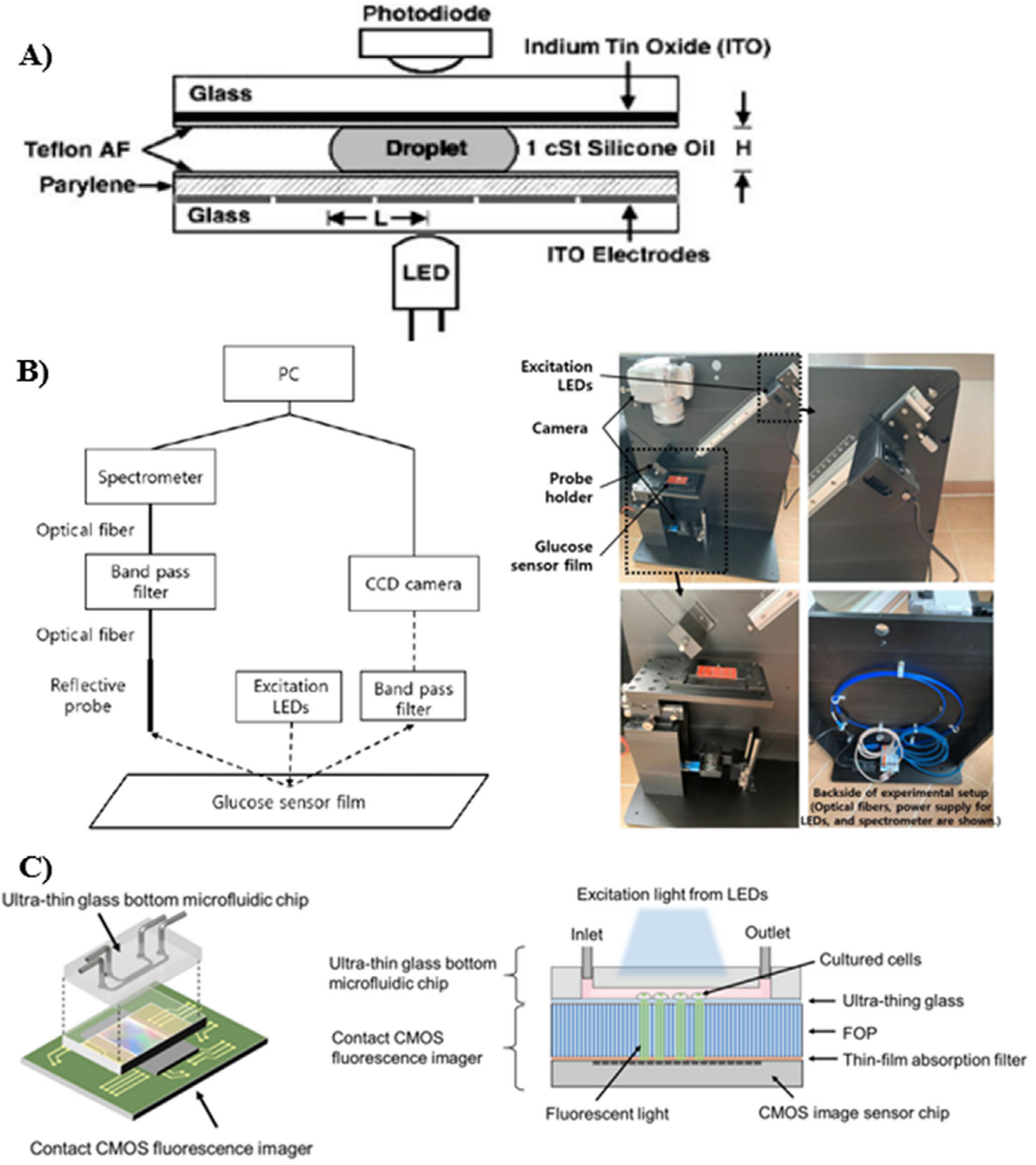

Figure 5. A) Vertical cross-section of the electrowetting chip, along with the optical detection instrumentation for absorbance glucose detection. Reproduced from[26] with permission from Elsevier. Copyright 2004, Elsevier. B) Schematic of a general optical detection system of a luminescence-based glucose sensor presented by Park et al.[27] Excitation light is provided by LEDs and filtered by a band-pass filter before reaching the glucose sensor film. The luminescent light is collected by an optical probe and analyzed by a spectrometer, while a CCD camera can be used for image detection.[27] Reproduced from with permission from MDPI, under a Creative Commons Attribution (CC BY) license. Copyright 2021, MDPI. C) Illustration of a fluorescence imaging system based on a contact CMOS chip. The ultrathin glass microfluidic chip contains cultured cells, where excitation light is emitted by LEDs. The fluorescent light is captured by the CMOS image sensor, which is in direct contact with the structure, allowing for high-efficiency optical detection.[63] Reproduced from[63] with permission from AIP, under a Creative Commons Attribution (CC BY) license. Copyright 2017, AIP.

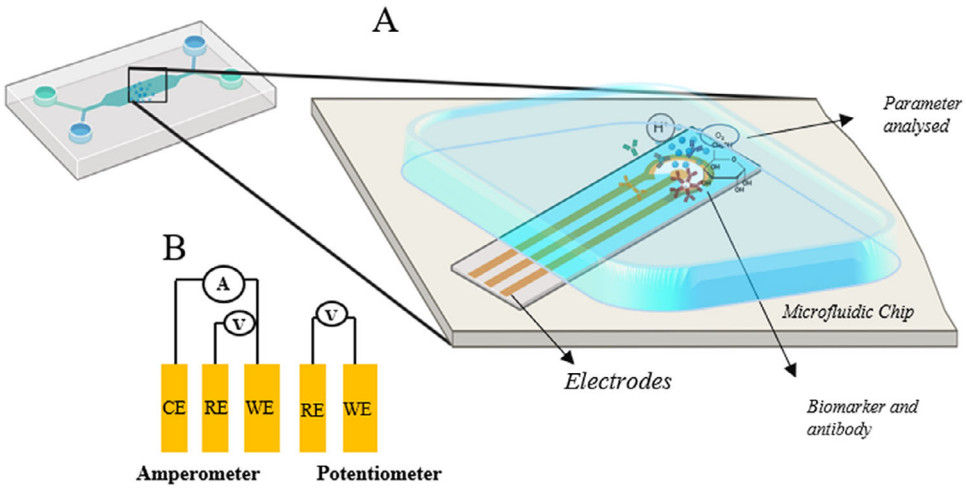

Figure 6. A) Schematic representation of a microfluidic chip integrating electrochemical sensors for analyte detection. The system consists of a microfluidic channel with embedded electrodes, where specific biomarkers interact with immobilized antibodies, generating an electrochemical signal. B) Diagram illustrating the working principles of potentiometric and amperometric measurements using a two or three-electrode system, respectively. Working Electrode (WE), Reference Electrode (RE), and Counter Electrode (CE).

with a detection limit of 20 µM and a dynamic range of 0.06–1 mM, allowing a noninvasively study.[30] The authors used, for the optical reaction, the enzymatic product NADH (nicotinamide adenine dinucleotide + hydrogen), converted due to lactase catalysation, that emits fluorescence at 460 nm when excited at 360 nm.

Apart of glucose and lactate, Takehara et al.[63] implemented contact fluorescence microscopy in a microfluidic chip to control the Endothelial growth factor and other biological samples. The proposed transducer is composed by a CMOS image sensor chip, fabricated using the 0.35 µm 2-poly, 4-metal standard CMOS technology, a thin-film absorption filter, and a fiber optic plate (FOP) (Figure 5C).

In summary, these studies demonstrate the variety of optical approaches used for monitoring key metabolic analytes such as glucose and lactate in microfluidic and OoC platforms. Each method offers distinct advantages and limitations, which must be considered depending on the required detection sensitivity, integration constraints, and long-term monitoring needs. Absorbance-based glucose detection methods are attractive due to their simplicity, low cost, and ease of integration with microfluidic chips. However, they typically require higher analyte concentrations and offer limited sensitivity compared to fluorescence or NIR spectroscopy. Luminescent and fluorescence-based methods provide higher sensitivity and lower LODs (0.1–0.5 mM), enabling continuous monitoring even at low analyte levels, but involve more complex optical setups (light source, filters, detectors) and may suffer from photobleaching and signal drift over long experiments. NIR spectroscopy offers the advantage of label-free detection, reducing chemical interference and enabling non-invasive measurement, but its integration into miniaturized OoC systems remains technically challenging due to alignment, signal-to-noise ratio, and cost of components. Photoacoustic methods, while promising for high accuracy and non-invasiveness, are still in an early stage of miniaturization and have not yet been widely adopted in OoC platforms.

3.2. Electrochemical Transducers

Comparing with optical detection, electrochemical detection is more favorable to miniaturization; the electrical signal is already available at the transducer's output.[65]

Electrochemical sensors have been of much interest due to their easy integration in microfluidic devices. They allow multiparametric monitoring of metabolites by multiplexed sensors, and their architecture makes this method robust and reproducible for in situ monitoring.[10,24] In the electrochemical sensors, the sensing surface can be composed only by metal electrodes, which is mostly used for pH sensors.[15,66] However, most of the parameters to be analysed need a biomarker, as frequently used for glucose and lactate detection.[67,68] As demonstrated in **Figure 6**, in a potentiometric electrochemical sensor, it is measured the difference of the potential between the reference electrode (RE) and the working electrode (WE). The metal oxide based (MOx) sensors and ion-sensitive field-effect transistors (ISFETs – which resemble a regular metal oxide silicon FET where the metallic gate was changed by an ion-selective membrane) are some examples of potentiometric sensors,[6,10] being the latter specially targeted for miniaturization and integration. In amperometric sensors, usually a third electrode is needed, the counter electrode (CE), for measuring changes in the current flowing between the electrodes due to the electrically active species.[6] Apart of these analysed parameters and transducer type, some analytes can be detected by an impedimetric transducer, which measure the electric impedance of a solution.[13,69] **Table 2** presents a variety of electrochemical transducers and their biological parameter detection, such as pH, oxygen, glucose, lactate, etc.

3.2.1. pH Detection

Electrochemical pH sensors presented in the literature rely mostly on the potentiometric type, i.e., the variation of the

Table 2. Comparison of electrochemical methods and transducers toward integration in LoC/OoC platforms.

	Parameter	Detection Method	Transducer	Sensitivity	LOD	Applications
[15]	pH	Potentiometric	RuO_2 nanorods	0.058 V pH^{-1}	(2–10) ±0.05	hypoxic cardiomyocytes study
[71]	pH	Potentiometric	Thin Pt film and Si_3N_4	0.039 V pH^{-1}	NR	Cellular behavior
[66]	pH	Potentiometric	Thin film IrOx	0.063 V pH^{-1}	NR	Human tumor cell (Brain) cultures
[67]	pH	Potentiometric	Thin film IrOx	0.0585 V pH^{-1}	NR	Cell culture/toxicity studies
[72]	pH	Potentiometric	ISFET (Ta_2O_5 gate)	0.056 V pH^{-1}	0.002 pH	Cell culture
[73]	pH	Amperometric	FG-FET (TiO_2 gate)	1.5305 µA pH^{-1} (7–9) 1.3574 µA pH^{-1} (4–7)	0.1 pH	Organ modules and biological monitorization
[71]	O_2	Amperometric	Bare Pt structures	100 pA/O_2%	NR	Cellular behavior
[68]	O_2	Amperometric	Pt	0.58 µA $cm^{-2}µM^{-1}$	1 µM	Drug screening and toxicity studies; organ-on-a-chip systems
[66]	O_2	Amperometric	Thin film Pt	0.735 µA $µM^{-1}cm^{-2}$	NR	Human tumor cell (Brain) cultures
[67]	O_2	Amperometric	Thin film Pt	NR	NR	Cell culture/toxicity studies
[72]	O_2	Amperometric	Pt electrode	3.7 nA per mg L^{-1}	NR	Cell cultivation
[86]	O_2	Amperometric	Pt	−0.595 nA kPa^{-1}	0.1 kPa	Tumor hypoxia
[74]	O_2	Clark-type	Pt electrode	−0.121 µA $cm^{-2}µM^{-1}$	0.2 µM	Cellular respiration (Organ on a chip)
[66]	Glucose and lactate	Amperometric	Pt electrode	3.3 nA $mM^{-1}mm^{-2}$ (Glucose) 2.6 nA $mM^{-1}mm^{-2}$ (Lactate)	75 µM (glucose) 90 µM (lactate)	Human tumor cell (Brain) cultures
[67]	Glucose and lactate	Amperometric	Pt electrode with CoPC	6 nA mM^{-1} (Glucose) 5 nA mM^{-1} (Lactate)	5 mM (Glucose) 1 mM (Lactate)	Cell culture/toxicity studies
[76]	Glucose	Amperometric	Carbon Paste	I (A) = 75.43c (mM) +1.31	NR	Liver-on-a-chip
[75]	Glucose	Amperometric	n-type conjugated polymer	NR	1 nM	Research in organic bioelectronics and microfluidics
[68]	Glucose and lactate	Amperometric	Pt electrode	3.80 nA mM^{-1} (Glucose) 10.77 nA mM^{-1} (Lactate)	7.6 µM (Glucose) 6.1 µM (lactate)	Drug screening and toxicity studies; organ-on-a-chip systems
[78]	Glucose and lactate	Amperometric	Pt electrode	NR	NR	Liver-on-a-chip
[77]	Glucose and lactate	Amperometric	Pt/Ir electrode	19.8×10^3 nA $mM^{-1}cm^{-2}$ (Glucose) 8.5×10^2 nA $mM^{-1}cm^{-2}$ (Lactate)	1.1 mM (Glucose) 0.6 mM (Lactate)	Cartilage-on-a-chip
[69]	Respiratory movements of the cell	Impedimetric	Copper electrode	NR	NR	Lung-on-a-chip
[80]	Cell growth	Impedimetric	Graphene electrodes	NR	NR	Neural cells in organ-on-a-chip
[33]	Toxicity	TEER	ITO Electrodes	NR	NR	Lung cancer-on-a-chip
[79]	IFN-γ	Amperometric	Gold electrodes	0.0023 pg mL^{-1}	6 pg mL^{-1}	Point-of-care biosensing platform
[72]	Biomass concentration	Amperometric	Platinum	0.65% per g L^{-1} biomass	NR	Cell culture
[84]	Hg(II)	TEER	Ag/Cl electrodes	1.78 µA nM^{-1}	0.1 nM	Gut-on-a-chip
[85]	Reactive oxygen species	TEER	Gold electrodes	NR	NR	Placenta-on-a-chip

NR- Not Reported

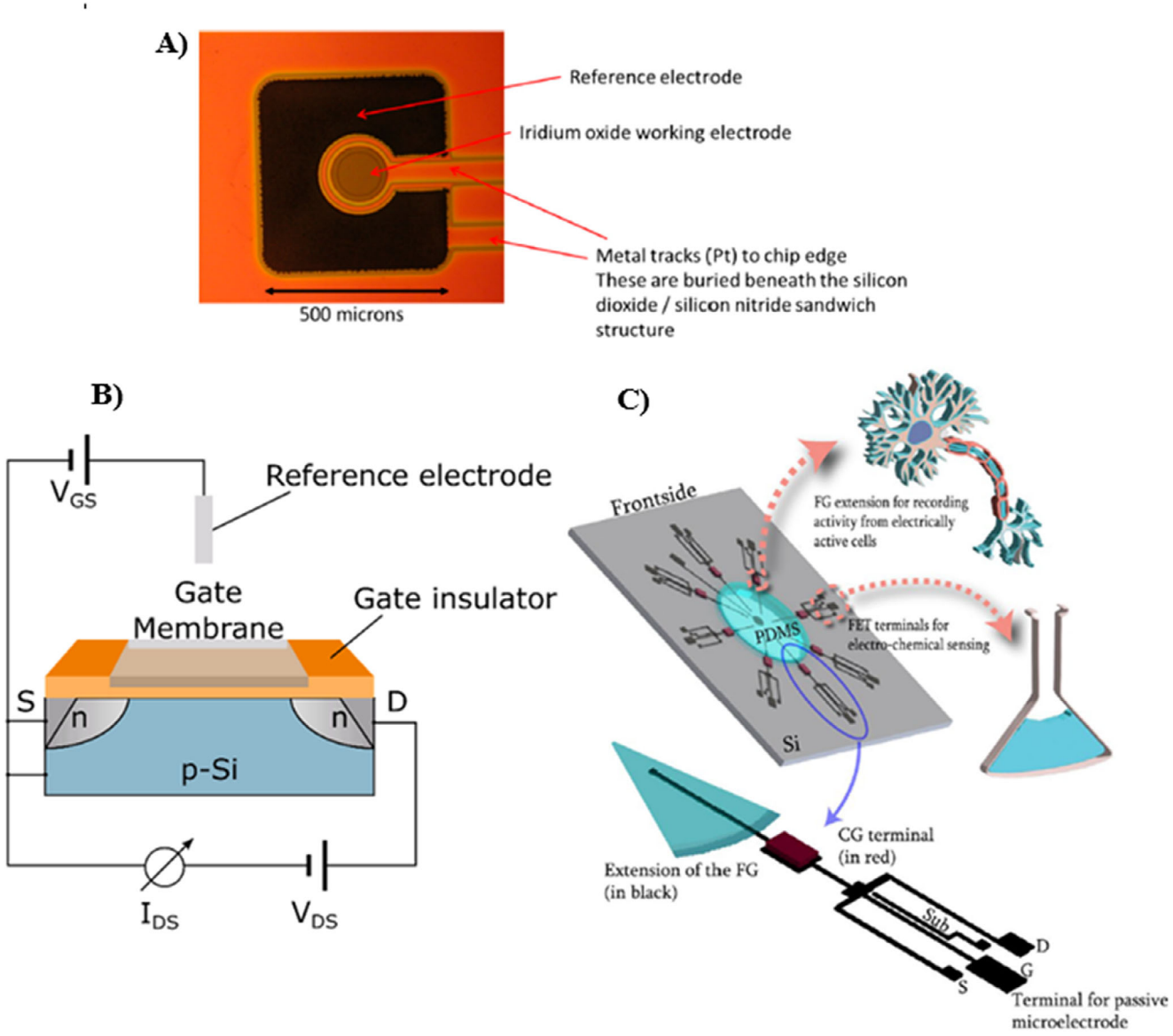

Figure 7. A) Optical image of the sensor of Pemberton et al., showing the reference electrode, iridium oxide working electrode, and platinum metal tracks embedded beneath the silicon dioxide/silicon nitride structure. Reproduced from[67] with permission from MDPI, under a Creative Commons Attribution (CC BY) license. Copyright 2014, MDPI. B) Schematic representation of an ISFET, illustrating the p-type silicon substrate, gate insulator, floating gate membrane, and reference electrode used for potentiometric electrochemical sensing. Reproduced from[10] with permission of ACS Publications, under a Creative Commons Attribution (CC BY) license. Copyright 2021, ACS Publications. C) Schematic of the proposed OoC device by Aydogmus et al.[73] Pink arrows indicate electrical connections for floating-gate FETs used to monitor pH changes, as well as extension of the floating-gates used as microelectrodes for recording activity from electrically active cells. In the purple arrow is an inset of one of the sensors with the labeled terminals.[73] Reproduced from[73] with permission from Nature, under a Creative Commons Attribution (CC BY) license. Copyright 2024, Nature.

electrical potential parameter is measured as a function of the pH H^+ ions.[70] In the developed pH sensor, Bonk et al.[71] used Pt structures passivated by a thick 1.2 µm layer of silicon nitride (Si_3N_4). Thin Si_3N_4 layers (20 or 60 nm) were used as the sensitive material of the pH electrodes. These electrodes showed a linear behavior in the pH range from 4 to 9, with a sensitivity of up to 39 mV per pH step. Also, Weltin et al.[66] presented a human tumor cell culture system with a potentiometric pH sensor. Five pH sensors were used, based on thin-film iridium oxide electrodes. The pH sensors presented a linear sensitivity of 63 mV pH^{-1}.[66] Similarly, Pemberton et al. developed a potentiometric electrochemical sensor based of iridium oxide layers for the WE (**Figure** 7A).[67] The authors achieved a sensitivity of 58.5 mV pH^{-1}, a rapid response (< 1 min) to pH changes and a drift less than 0.01 pH.[67] Apart of Pt with Si_3N_4 and IrOx, also Ruthenium Oxide (RuOx) is frequently used for the WE of the potentiometric pH transducers. In[15] Tanumihardja et al., it is used RuOx nanorods as sensing material. The authors used two-electrodes configuration, with the Ag/AgCl reference electrode placed 5 mm from the RuOx working electrode. The sensor

achieved a sensitivity of 58 mV pH^{-1}, as the sensor reported by Pemberton et al.[67] in a pH range of 2–10 with 0.05 pH variations.

Krommenhoek et al. also reported a potentiometric pH sensor, based on an ISFET (Figure 7B).[10,72] The gate of Ta_2O_5 oxide is in direct contact with the electrolyte surrounding the sensor, allowing hydrogen ions in the solution to interact with the Ta_2O_5 oxide. Consequently, the surface charge of the gate oxide varies with the concentration of hydrogen ions in the solution, enabling the threshold voltage of the device to serve as a reliable measure of the solution's pH. The authors achieved a sensitivity of 56 mV pH^{-1}.[72] Also based on a FET, Aydogmus et al.[73] developed an amperometric pH sensor (Figure 7C). Compared to the ISFET studied by Krommenhoek et al.,[72] this transistor responds to charge accumulation on the floating gate of the FET (FG-FET), generating a proportional current,[73]rather than dependent of threshold voltage.[72] The selective layer used on the gate is of TiO_2. The developed FG-FET achieved worst sensitivity and a higher limit of detection than the ISFET, as reported in Table 2.

Overall, the studies described a variety of electrochemical strategies available for pH monitoring in OoC systems. While all aim to provide accurate and real-time measurements, their performance and suitability strongly depend on the electrode material and sensing method.

ISFET-based sensors provide better resolution (< 0.1 pH), miniaturization potential, and compatibility with CMOS fabrication, which facilitates integration. Regarding metal oxide electrodes, the IrOx offers higher sensitivity and good stability over a broad pH range when compared to Pt thin films, making them a popular choice, but their deposition processes is less compatible with soft microfluidic materials.

3.2.2. Oxygen Detection

Amperometric measurements have been widely employed in oxygen detection using electrochemical transducing systems. In particular, most of the works published in the literature report circular platinum electrodes in the inlet and/or outlet inside the cell culture chamber.[66,68,71] Based on that, Weltin et al.[66] implemented five circular oxygen platinum sensors, with 100 µm diameter, in a chamber for culturing T98G human brain cancer cells. Supported on 3 electrodes configuration, a potential of 800 mV was applied to promote the formation of platinum oxide. Subsequently, two successive negative potential steps (−350 and −300 mV) were applied to reduce the oxide and facilitate oxygen reduction, while the corresponding current was recorded.[66] The authors achieved a sensor with a sensitivity of 0.735 µA $\mu M^{-1}cm^{-2}$ in a medium with no CO_2 dependence. Dornhof et al.[68] also implemented a circular oxygen sensor with 200 µm of diameter inside of culture channels. The authors developed three platinum sensors in each of three microchannels. The fabricated sensor presented a sensitivity of −0.58 µA $cm^{-2}\mu M^{-1}$ with a relative error of 0.8% ± 0.4% before and 1.2% ± 0.4% after long-term measurement. A limit of detection below 1 µM was observed. By implementing cell cultures in the channels and measuring the oxygen content in the inlet and outlet of the channels, this approach allowed the authors to measure oxygen consumption rates very precisely and to reveal drug-induced effects on respiratory metabolism.[68]

A microelectrodes array was also proposed for oxygen sensing. For instance, Pemberton et al.[67] used a sensor with 3 microelectrodes composed by a working Pt microelectrode array with six discs of 10 µm diameter, an electroplated Ag/AgCl reference electrode (1500 µm × 400 µm), and a Pt counter electrode (1500 µm × 400 µm), as shown in **Figure** 8A. The authors studied the disc diameter in the sensor response and concluded that 10 µm is the minimum diameter that meets the requirements, as it exhibits the steady-state behavior typical of microelectrodes and provides a reproducible steady-state current response.[67] Other O_2 sensor with 114 microelectrodes with 4 µm of diameter was designed by Krommenhoek et al.[72] The experimental results with supernatant solution indicated that the current flowing through the microelectrodes array change linearly with the concentration of dissolved oxygen, resulting in a sensitivity of 3.7 nA $mg^{-1}L^{-1}$. A low current was obtained in the absence of oxygen, demonstrating the high selectivity of the sensor.[72]

For the dissolved oxygen measurements, the Clark-type amperometric sensors have been commonly used. Based on this architecture, Liebisch et. al.[74] developed a three-electrodes sensor for dissolved oxygen measurements. As presented in Figure 8B, the sensor is composed of a Pt WE, an Ag/AgCl RE and a Pt CE. In a Clark-type sensor, a gas-permeable membrane separates the sensor electrolyte from the measurement medium to eliminate cross-sensitivity issues. The authors applied a fixed potential between the working electrode and the reference electrode, forcing the reduction of dissolved oxygen. The counter electrode serves to balance the system and prevent the net consumption of oxygen in the solution. The generated current is measured at the working electrode, resulting in a sensor with a sensitivity of −0.121 µA $cm^{-2}\mu M^{-1}$ and a resolution of 0.2 µM.[74]

When compared, these studies highlight the versatility of electrochemical oxygen sensors for integration in OoC platforms. Clark-type electrodes remain the most widely used approach due to their high sensitivity and well-established operation principles. However, they consume oxygen during measurement, which can alter the local concentration in small-volume OoC environments and consequently affect biological responses. Microelectrode-based designs minimize this issue by reducing sensor size and response time, but their small dimensions make them more prone to drift, biofouling, and fabrication variability. Integration with CMOS readout circuits provides additional advantages in size, cost, signal stability, and multiplexing capabilities, though at the more complex microfabrication.

3.2.3. Glucose, Lactate and Others Analytes Monitoring

Glucose and lactate have also been detected and monitored using electrochemical biosensors,[66] mostly by means of amperometry measurements. In sensing, the most used elements for biorecognition were the glucose oxidase (GOX) and the lactate oxidase (LOX) enzymes, which react with glucose and lactate analytes, respectively.[66,67,75–77] As presented in Table 2, the analysed glucose and lactate biosensors primarily use Pt electrodes[66,68,78] or variations, such as Pt/Ir[77] or mediators like cobalt phthalocyanine (CoPC).[67] For instance, Bavli et al.,[78] Dornhof et al.[68]

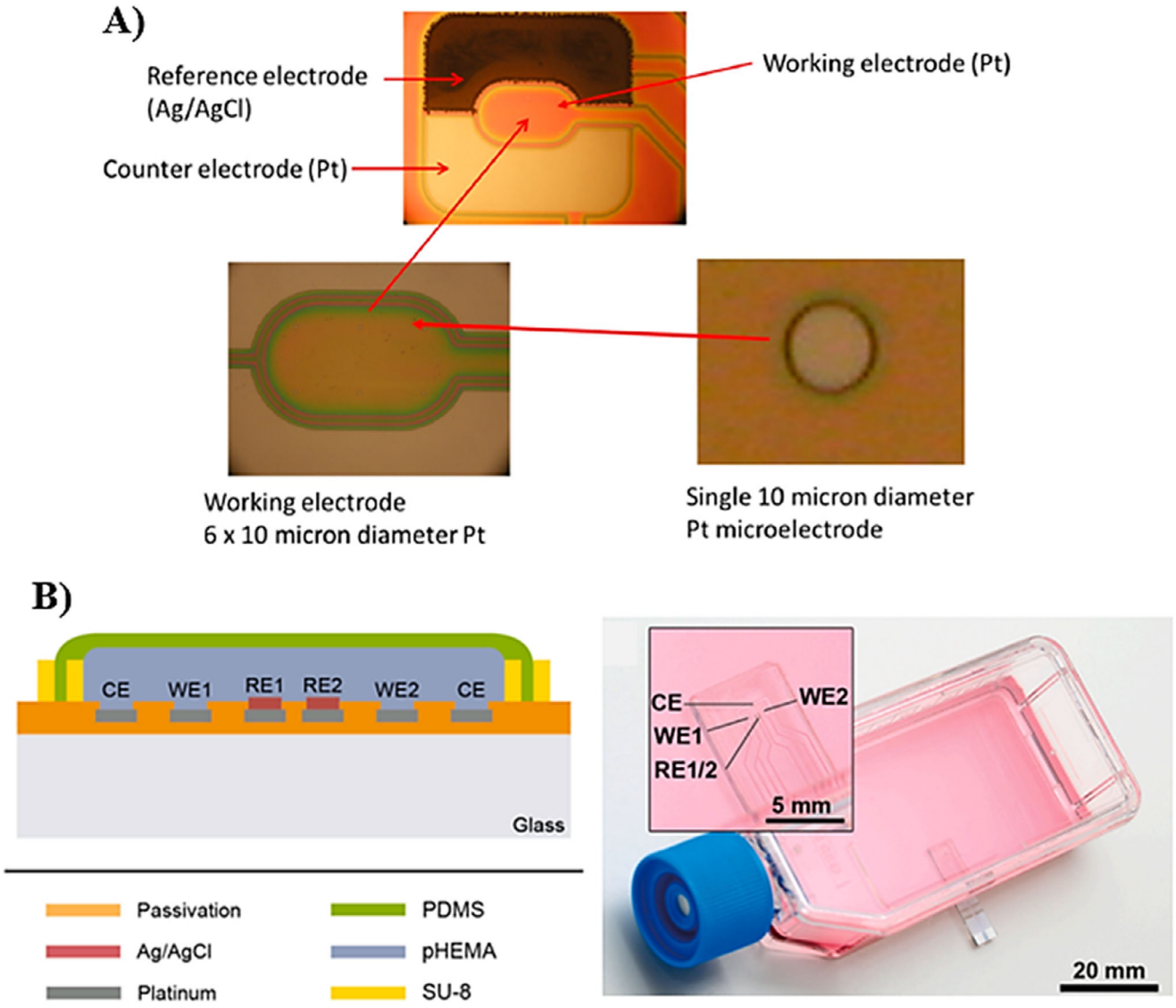

Figure 8. A) Photograph of a microfabricated oxygen sensor from Pemberton et al.[67] showing bare platinum working and counter electrodes; working electrodes = 6 off 10 micron diameter. Reproduced from[67] with permission from MDPI, under a Creative Commons Attribution (CC BY) license. Copyright 2014, MDPI. B) Schematic representation of the clark-type microsensor architecture from Liebisch et al.,[74] showing the counter electrode (CE), working electrodes (WE1, WE2), and reference electrodes (RE1, RE2) embedded in a glass substrate. Different materials used in the fabrication are highlighted, including platinum, Ag/AgCl, PDMS, pHEMA, and SU-8. The microsensor chip was embedded in a conventional tissue culture flask. The inset provides a detailed view of the Clark-type microsensor. Reproduced from[74] with permission from ELSEVIER. Copyright 2020, ELSEVIER.

and Weltin et al.[66] designed transducers based in Pt electrodes. Dornhof et al.[68] achieved a sensitivity of 3.80 nA mM^{-1} for glucose and 10.77 nA mM^{-1} for lactate,[68] higher values were obtained by Weltin et al., with 3.3 nA $mM^{-1}mm^{-2}$ for glucose and 2.6 nA $mM^{-1}mm^{-2}$ for Lactate.[66] Furthermore, the authors also achieved a better resolution for both analytes, namely 7.6 and 6.1 µM, for glucose and lactate, respectively.[68] With a variation of the traditional Pt electrodes to CoPC electrodes,[67] (**Figure 9A**), Pemberton et al. proposed a glucose biosensor with a sensitivity of 6 nA mM^{-1} and a lactate biosensor with 5 nA mM^{-1} sensitivity. The LOD obtained was 5 mM for glucose and 1 mM for lactate.

Rothbauer et. al.[77] designed a glucose and a lactate biosensor based on 3-electrodes configuration integrated in a cartilage-on-a-chip, with a working electrode of Pt/Ir, as depicted in Figure 9B.[77] The biosensors were characterized applying a 0.75 V potential. The authors obtained a sensitivity of 19.8 × 10^3 nA $mM^{-1}cm^{-2}$ (glucose) and 8.5 × 10^2 nA $mM^{-1}cm^{-2}$ (lactate),[77] which is a higher sensitivity when compared to the other electrochemical glucose biosensors described in Table 2. However, the obtained limit of detection, which was 1.1 mM for glucose and 0.6 mM for lactate, is worse than when using Pt-based electrodes in the biosensors.[66,68]

Other materials have been widely used for glucose detection. Wu et al.[76] used carbon paste and silver (Ag) for the working and counter electrode, respectively, and silver chloride for the reference electrode on a Polyethylene Terephthalate (PET) substrate

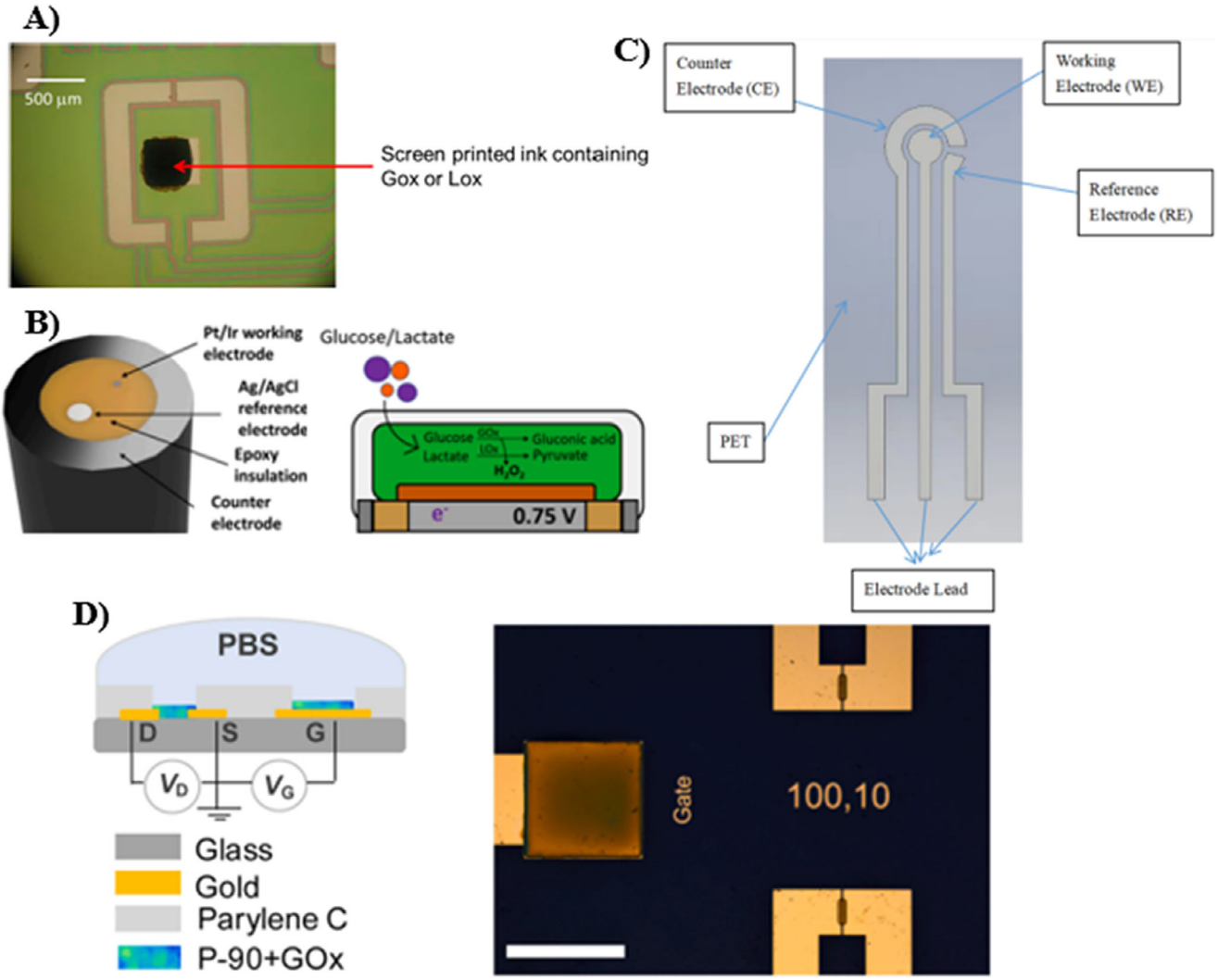

Figure 9. A) Photograph of the microfabricated screen-printed microbiosensor showing the depositon of the screen-printed working electrode ink, from Pemberton et al.[67] Reproduced from[67] with permission from MDPI, under a Creative Commons Attribution (CC BY) license. Copyright 2014, MDPI. B) Cartilage-on-a-chip platform with integrated biosensor, from Rothbauer et al.,[77] including cross-sectional view of the sensor wire and sensor tip coating. Glucose and lactate are oxidized in the sensor tip by GOx and LOx. Reproduced from[77] with permission from ELSEVIER, under a Creative Commons Attribution (CC BY) license. Copyright 2025, ELSEVIER. C) Design of the electrochemical sensor from Wu et al.[76] Reproduced from[76] with permission from E3S Web Conf. Copyright 2020, E3S Web Conf. D) Schematic from Koklu et al. of the OECT with the electrical connections from the left, and a microscope image of the gate along with two channels from the right.[75] The enzyme (GOx) was immobilized on P-90, patterned at the channel and on the gate electrode.[75] Reproduced from[75] with permission from ELSEVIER. Copyright 2021, ELSEVIER.

(Figure 9C).[76] Koklu et al.[75] integrated a n-type organic electrochemical transistor (OECT) in a microfluidic device.[75] The GOX enzyme was immobilized on P-90, as shown in Figure 9D.[75] This method for glucose detection presented a lower detection limit than those reported in Table 2. According to the authors, the transducer exhibits high sensitivity to low glucose concentrations, ≈1 nM, demonstrating that n-type organic electrochemical transistors stand out as next-generation miniaturized biosensors and will be useful for fundamental studies and applied research in organic bioelectronics and microfluidics.[75]

Among the various electrochemical biosensing approaches, distinct performance trends can be observed. Pt-based electrodes remain the most widely used due to their excellent stability, reproducibility, and biocompatibility, offering good sensitivities and low detection limits in the micromolar range. The carbon-based materials, such as carbon paste and printed Ag/AgCl systems, stand out for their low fabrication cost and high adaptability to polymeric substrates, though typically with reduced sensitivity and signal-to-noise ratio. The most promising recent advances are OECTs, which combine exceptional sensitivity down to the nanomolar range, high miniaturization potential, and compatibility with low-cost fabrication and a green environment.

Other biological parameters were also detected and monitored in organ-on-a-chip systems based on electrochemical transducers. Liu et al.[79] developed a microfluidic chip integrated with magnetic beads (MBs) for continuous monitoring of Interferon gamma (IFN-γ) concentration.[79] (IFN-γ) is a key proinflammatory cytokine with antiviral, antiproliferative, and

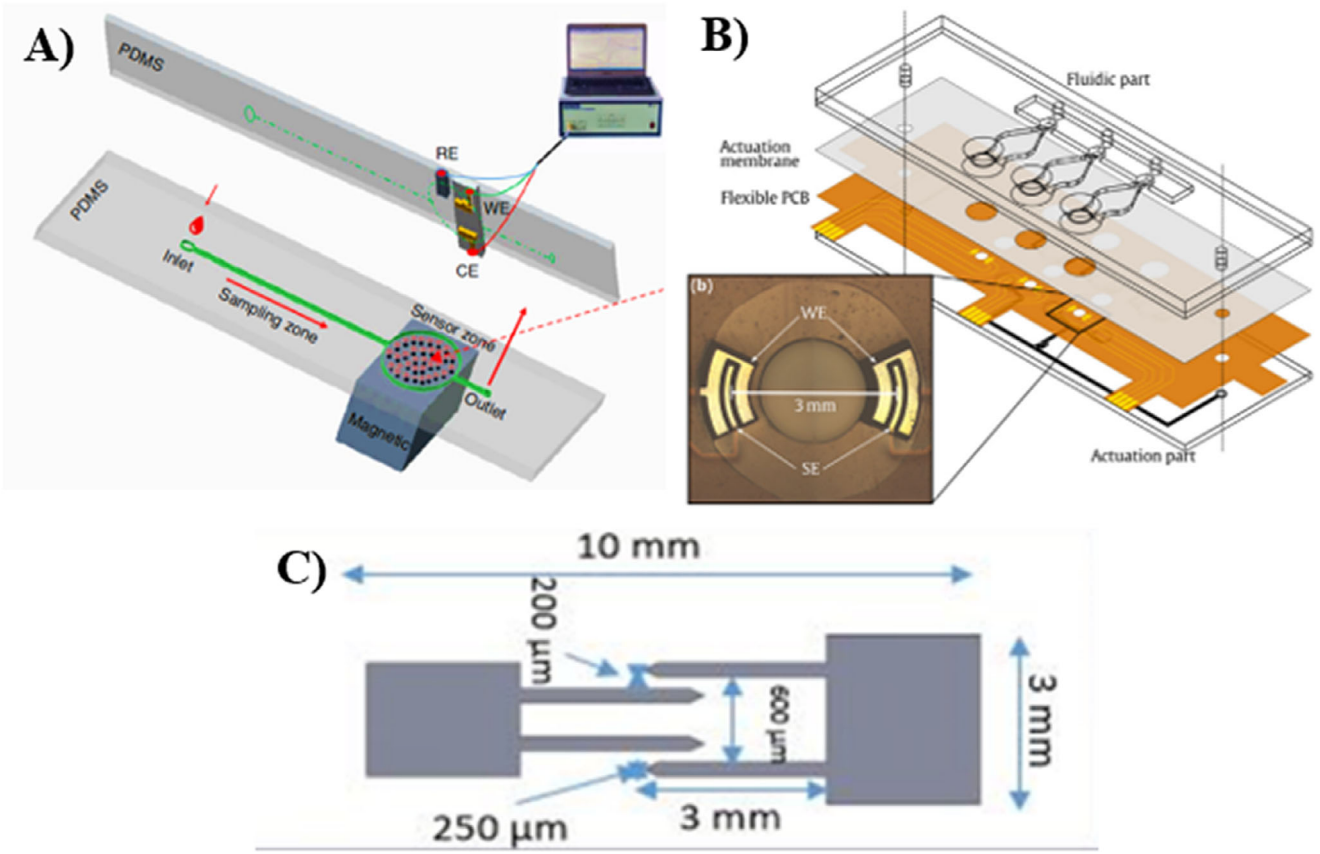

Figure 10. A) The schematic of the integrated customized microfluidic chip where it can be seen the sampling zone and the sensor zone; the sensing electrodes, including the working electrode (WE), reference electrode (RE), and count electrode (CE), on the silicon wafer, are integrated in the the top part of a PDMS-based chip, from Liu et al.[79] Reproduced from[79] with permission from Nature, under a Creative Commons Attribution (CC BY) license. Copyright 2019, Nature. B) Design of the microimpedance transducer and integration in the lung-on-a-chip from Mermoud et al.[69] The lung-on-a-chip proposed consists of a flexible PCB bonded between the actuation part and the actuation membrane of the lung-on-a-chip. Each sensing region consists of a tetrapolar arrangement of two pairs of electrodes separated by a distance of 3 mm. The sensing electrodes (SE) of each pair are located in the centre of the working electrodes (WE) to avoid zones of negative sensitivity.[69] Reproduced from[69] with permission of ELSEVIER. Copyright 2018, ELSEVIER. C) Schematics and dimensional characteristics pertaining to the interdigitated electrode (IDE) structure from Ouedraogo et al.[80] Reproduced from[80] with permission from APL Materials, under a Creative Commons Attribution (CC BY) license. Copyright 2025, APL Materials.

immunoregulatory functions. Elevated IFN-γ levels can serve as an early marker for diseases such as tuberculosis, HIV, Crohn's disease, paratuberculosis, and various cancers.[79] Aptamers labeled with ferrocene (Fc), targeting IFN-γ, were immobilized on a three-electrode transducer consisting of two gold electrodes (WE and CE) and a silver reference electrode (RE) (**Figure 10A**).[79] The MB-aptamer solution flowed through the microfluidic device with a magnetic field applied, fixing the MB-aptamers in the sensor zone. The oxidation signal of ferrocene was measured via chronoamperometry, achieving a sensitivity of 0.0023 pg mL^{-1} and a detection limit of 6 pg mL^{-1}.[79] In a similar way, Krommenhoek et al.[72] used an amperometric method for biomass concentration monitorization using platinum electrodes. Mermoud et al.[69] developed a microimpedance tomography system integrated into a lung-on-a-chip to mimic the alveolar barrier and study the respiratory movements of the cells.[69] The system includes three impedimetric coplanar gold electrodes (Figure 10B), which monitor resistivity changes in real time and track the 3D movements of the membrane. The electrodes are arranged around a 2 mm opening, allowing the cell imaging, and are positioned 1 mm below the membrane to accommodate its 600 µm deflection. As represented in Figure 10 B, the transducer is composed by a working electrode to inject current, while sensing electrodes (SE) measure potential differences, enabling precise assessment of barrier integrity and mechanical behavior.[69] Also based in an impedimetric transducer, Ouedraogo et al.[80] developed a graphene-based sensor for real-time monitoring of neural cell growth in an organ-on-a-chip device.[80] This sensor comprises two electrodes, namely the working and counter electrodes, as illustrated in Figure 10C.[80] The closely spaced, finger-like structures within the electrode design increase the electrode-electrolyte interface area, thereby facilitating efficient electrochemical reactions and enhancing signal detection. Additionally, the interdigitated electrode configuration effectively minimizes capacitive coupling between adjacent fingers, reducing interference and noise that arises from stray capacitance.[80]

Based on electrical measurement, some authors implemented a trans-epithelial electrical resistance (TEER) sensor to study the bio-impedance of cells and monitoring barrier tissues development.[81] TEER is a key non-invasive method to assess

Table 3. Comparison of mechanical methods and transducers toward integration in LoC/OoC platforms.

Refs.	Parameter	Detection Method	Transducer	Sensitivity	LOD	Applications
[88]	KI solutions and detection of PS latex particles	Piezoelectricity	ZnO	NR	NR	Lab-on-a-chip
[95]	Blood Pressure	Pressure sensors	Fused Silica Capillary	NR	134.5 ± 0.3 mmHg 1.5 ± 0.2 mmHg	Body-on-a-chip
[89]	Contractile behavior	Piezoelectricity	PVDF film	NR	NR	Heart-on-a-chip
[92]	Circulating tumor cells	Piezoelectricity	Ceramic plate	NR	NR	Phenotyping of cancer cells
[91]	Cardiac contraction	Piezo-resistivity	CB:TPU	Gauge factor 2.56	NR	Cardiac micro-tissues
[93]	Detection of contractile stresses exerted by multiple microtissues	Resistive Strain Sensor	PBS (phosphate-buffered saline)	0.67 $\Omega\ Hz^{-1/2}$	$\Delta r \approx 50$ nm	Heart-on-a-chip
[94]	Evolution of the stiffness of cell-hydrogel	Resistive Strain Sensor	Carbon nanotube (CNT)	NR	NR	Cultured tissue constructs
[90]	Faster mixing microfluidic	Piezoelectricity	PZT / PVDF	NR	NR	Microfluidic devices
[87]	Mechanism of hydronephrosis	Resistive force sensor	Nano-sized force sensing material	NR	20 g to 10 Kg	Renal-on-a-Chip

NR- Not reported

epithelial barrier integrity and detect permeability changes caused by cell layer disruption.[82] This type of sensor has been applied in barriers-on-a-chip to study the integrity of organs models like skin, brain,[83] gut,[84] lung,[33] and placenta.[85] Khalid et al.[33] implemented an indium tin oxide (ITO) TEER sensor to study the toxicity of drugs. Using a similar sensor, Wang et al.[84] and Schuller et al.[85] implemented TEER sensors to study the cell barrier integrity in the study of Hg(II)[84] and reactive oxygen species.[85]

3.3. Mechanical Transducers

While molecule-based analysis techniques are relatively easy to apply into OoC systems, applying and measuring mechanical forces and displacement is more challenging due to the small volume and limited robustness of these platforms.[7] As a result, mechanical transducers are still underrepresented in OoC systems, being far less common than optical or electrochemical. Nevertheless, they are beginning to emerge in OoC models designed to replicate the dynamic movement of organs.[11,87] These movements, seen by cell mechanics, play a crucial role in various biological processes, influencing the fate and function of both cells and tissues. Tissue mechanical properties have consistently been shown to be a key factor in cell behavior and tissue morphogenesis. However, defining the ideal parameters for measuring these properties remains a significant challenge.[7]

The mechanical transducers in literature benefit from the advantages of some specifically materials properties, as piezoelectricity,[88–90] piezo-resistivity,[91] and resistive strain, as presented in **Table 3**. Sakamiya et al. designed a system to mimic the contractile behavior of the cardiac tissue,[89] taking advantage of piezoelectric material properties. Contractile behavior is one of the key features of cardiac function and plays an important role in assessing the efficacy and safety of drugs during the screening process.[89] The authors designed a system with a micro-pillars structure made of PDMS. These micro-pillars are embedded within a culture chamber. To detect the deformation of the micro-pillar array when the cardiac tissue contracts, a PVDF (Polyvinylidene fluoride) film was used, outputting electrical signals proportional to the intensity of contraction, which is given by $V_0 = A \times k \times h \times F/(\pi \times d^4)$ (**Figure 11A**), where h represents the height at which equivalent force of the cardiac contraction is applied; d is the diameter of the pillar; k is the piezoelectric voltage constant of the PVDF film, and A is a constant. Based on that, the authors proved that the voltage (V_0) increased with the applied force (F) and the output frequency was proportional to the input one.[89]

Furthermore, some pathologies modify the elastic properties of biological cells.[88] Gao et al. integrated a transducing system to produce acoustic waves in a microfluidic channel, in order to evaluate the elastic properties of fluids and single biological cells.[88] In this system, the authors presented two piezoelectric transducers, one working as an actuator and the other working as sensor. A Zinc oxide (ZnO) film was sinusoidally actuated at its resonance frequency, 1.3 GHz. This device allowed to characterize chemical solutions of different concentrations.[88] In addition, Zhao et al.[92] implemented a piezoelectric actuator to evaluate cell biophysical properties.[92] In this case, the authors used a piezoelectric ceramic plate, stimulated with a sinusoidal wave at 1.98 MHz. The transducer forms an acoustic resonance field in the main channel. The authors proved that, applying an acoustic force, the position of the cells when exciting the channel is dependent on their biophysical properties.[92] Based on a piezoelectric material as an actuator to produce acoustic waves, Catarino et al.[90] compared lead zirconate titanate (PZT) and β-PVDF materials as actuators in microfluidic systems. The goal of the study was to develop an actuator capable of generating acoustic waves to facilitate mixing time in microfluidic devices, while avoiding the use of pumps or moving parts.[90] The authors demonstrated that both PZT and β-PVDF transducer materials effectively enhanced mixing, resulting in significantly reduced mixing times for the complete reaction process—achieving reductions of over 90% for PZT and 80% for β-PVDF in an 8 mm × 7 mm cuvette.[90]

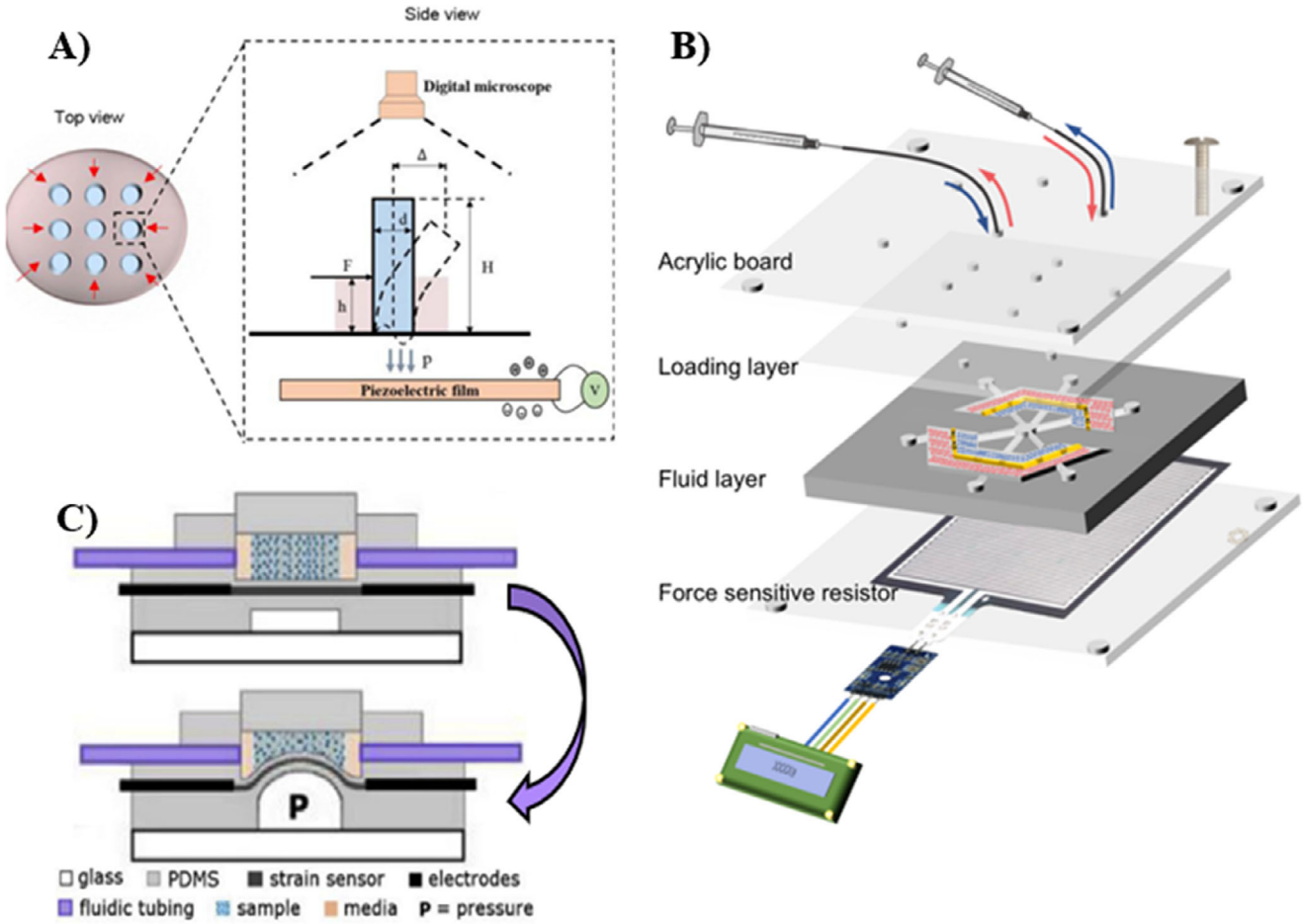

Figure 11. A) Detection of micro-pillar array deformation via digital image processing and piezoelectric sensing techniques from Sakamiya et al.[89] Reproduced from[89] with permission from ELSEVIER. Copyright 2020, ELSEVIER. B) Deformable membrane platform with on-chip strain sensors in compression mode of operation from Liu et al.[94] Reproduced from[94] with permission from ELSEVIER. Copyright 2018, ELSEVIER. C) Schematization of the Renal-on-a-Chip Microfluidic Platform with a Force-Sensitive Resistor from Xiao et al.[87] Reproduced from[87] with permission of ACS Publications. Copyright 2022, ACS Publications.

Taking advantage of the piezo-resistive materials properties, Lind et al. developed an instrumented cardiac microphysiological device.[91] The authors used thermoplastic polyurethane (TPU) ink filled with 25 wt.% carbon black nanoparticles (CB:TPU) to form an elastic piezo-resistive material with a Young's modulus of 8.8 MPa and resistivity of 1.19 Ω.cm.[91] The sensors discussed by Lind et al.[91] enabled non-invasive electronic readouts of the contractile forces generated by human stem cell-derived cardiac tissues. These sensors outputted a resistance change according to the contractile forces, demonstrating a gauge factor of 2.51 ± 0.09.[91] Also, Jayne et al.[93] developed a strain gauge sensor to monitor real-time mechanical deformation and force within PDMS structures in heart-on-a-chip devices. Each device featured a central cell culture well surrounded by an annular microfluidic channel. When a pressure differential is applied between the well and the channel, the separating PDMS wall deflects accordingly. This deflection alters the volume of the conductive phosphate-buffered saline (PBS)-filled microchannel, leading to a measurable change in the electrical resistance (ΔR). The resistance variation is directly correlated with the wall displacement, enabling the system to work as a transducer that converts mechanical strain into electrical signals. With proper calibration, this allows for accurate estimation of applied forces, whether externally induced or generated by the spontaneous contraction of the cardiac tissues.[93] This transducer presented a resistance variation of 0.67 Ω $Hz^{-1/2}$ and a maximum displacement variation of the wall of $\Delta r \approx 50$ nm.[93] Furthermore, Liu et al. used carbon nanotube (CNT) strain sensors applied in tissue engineering.[94] The electrical resistance of these sensors changes as the membrane deforms (Figure 11B), allowing the measurement of the stiffness of the tissue.[94]

Chen et al. designed capillary-assisted pressure sensors integrated into a microfluidic circulatory system.[95] The sensor is based on a simple physical principle without relying on electrical components. It uses air compression inside a capillary – an extremely thin tube with an internal diameter of 100 µm, made of fused silica. One end of the capillary is sealed with epoxy glue, while the other is inserted into a microfluidic channel where it is exposed to the fluid pressure. When the pressure in the channel changes, the air inside the capillary is compressed, causing a

Table 4. Comparison of temperature transducers toward integration in LoC/OoC platforms.

Refs.	Method	Transducer	Sensitivity	LOD	Applications
[38]	Resistive	Copper-constantan thermocouple wire	NR	150 °C	Liver-and-heart-on a- chip
[67]	Resistive	Platinum	0.2 Ω $°C^{-1}$	20–60 °C	Cell culture/toxicity studies
[25]	Resistive	Platinum	0.3542 mV $°C^{-1}$	35-45 °C	Efficiency of drug nanocarriers
[72]	Resistive	Platinum	2.2×10^{-3}/°C	20-45 °C	Cell culture
[99]	Resistive	Platinum	1695 ppm $°C^{-1}$	11 W (200 °C)	Lab-on-a-chip
[99]	Resistive	Platinum	1440 ppm $°C^{-1}$	245 °C	Lab-on-a-chip
[100]	Resistive	Aluminium	0.339 °C mA^{-1}	35-45 °C	OoC Device
[102]	Electronic (PTAT + relaxation oscillator)	0.18 µm CMOS IC	57.1 ns $°C^{-1}$	25 – 100 °C	OoC Device

displacement of the liquid–gas interface. This movement is observed through a microscope coupled with a CCD camera. It was demonstrated that the sensor can detect rapid pressure changes, such as simulated pulsations, and that it maintains a stable performance over several days in an incubation environment at 37 °C and high humidity, with a maximum pressure of 134.5 ± 0.3 mmHg and a minimum pressure of 1.5 ± 0.2 mmHg.[95] Furthermore, Xiao et al.[87] constructed a force-sensitive resistor integrated in a Renal-on-chip Microfluidic platform Figure 11C. The sensor responded to force applied to the sensing are, with a sensitivity from 20 g to 10 Kg. The sensor is composed by a robust polyester film, a high-conductive material, and a nano-sized force sensing material. The top layer contained the force-sensitive area on a flexible film, while the bottom layer had conductive circuit traces on another flexible film. These two layers were bonded with a spacer adhesive, except in the active area. When force was applied to this area, the top force-sensitive layer contacted the bottom conductive traces, causing a change in resistance at the output terminals.[87]

Overall, these examples underline the growing interest in mechanical transducers for OoC platforms, particularly for applications involving shear stress, pressure regulation, or tissue mechanics. Although their use is less widespread, mechanical sensing and actuating offer the unique advantage of directly probing physical stimuli relevant to the dynamic cell behavior and tissue function.

Piezoresistive sensors are attractive due to their simple electrical readout, higher sensing range, and higher sensitivity. However, they often require careful calibration to minimize temperature-dependent drift and careful fabrication.[96] Piezoelectric sensors, on the other hand, is a simpler structure, but their integration into soft, flexible OoC materials can be more challenging. Capacitive and strain gauge-based sensors provide good mechanical compliance and can be embedded in flexible chips, though they may be more sensitive to noise and environmental fluctuations.

3.4. Resistive transducers

Temperature needs to be carefully monitored in mostly organ-on-a-chip devices. For that, it is necessary to implement accurate and sensitive sensors and actuators to maintain the cells in a suitable environment to growth.[97] As presented in **Table 4**, platinum is the most used metal for temperature transducers, due to its high temperature coefficient of resistance (TCR) value, chemical stability, high conductivity, good adhesion to substrates, and biocompatibility, which makes it increasingly used and sought-after for biomedical applications, particularly in organ-on-a-chip systems.[25,67,72,98,99] Pemberton et al. implemented a platinum resistance temperature sensor (**Figure 12A**) with a linear resistance over the range 20–60 °C. The authors obtained a sensor with a sensitivity of +0.2 Ω $°C^{-1}$.[67] Furthermore, Sousa et al. obtained a platinum resistance temperature detector (RTD) with a resolution of 0.1 °C in the range of physiological (35 °C) to hyperthermia (45 °C) temperatures. The authors designed a four-wire configuration RTD, with 24 windings, 200 nm platinum film thickness, 10 µm of line width and spacing, and an area of 0.38 mm^2 (Figure 12B). Similarly, Krommenhoek et al. designed a resistance temperature sensor with a 150 nm thick platinum strip with a length of 4600 µm and a width of 10 µm.[72] The platinum sensor resistance at room temperature equals 486 Ω, and its TCR is 2.2×10^{-3} /°C.[72] Resnik et al.[99] also integrated a platinum heater having a TCR of 1695 ppm and a power consumption of 11 W to reach 200 °C.[99] Furthermore, the authors also integrated Pt temperature sensors with a TCR of 1450 ± 100 ppm.[99]

Regarding heating systems and their actuation, based on an aluminium transducer, Ferreira et al.[100] implemented a heating system in an OoC device. The authors studied three different geometries of aluminium microheaters (Figure 12C). The best geometry chosen by the authors presented a sensitivity of 0.339 °C mA^{-1}, and combine good temperature uniformity in a culture chamber with low power consumption (lower than the 1 W).[100] Using an identical geometry, Ferreira et al. also studied, through COMSOL Multiphysics numerical simulations, the best materials to use as microheaters in an OoC chamber.[101] The authors found that, for the same current consumption, a platinum microheater reached higher temperatures than an aluminium microheater. However, the aluminium microheater showed better results in terms of heat distribution uniformity. A silicon substrate and platinum microheater were found as the best combination for the microheater fabrication, featuring good heat distribution uniformity and lower current consumption.[101] In addition, the use of silicon instead of glass also allowed the

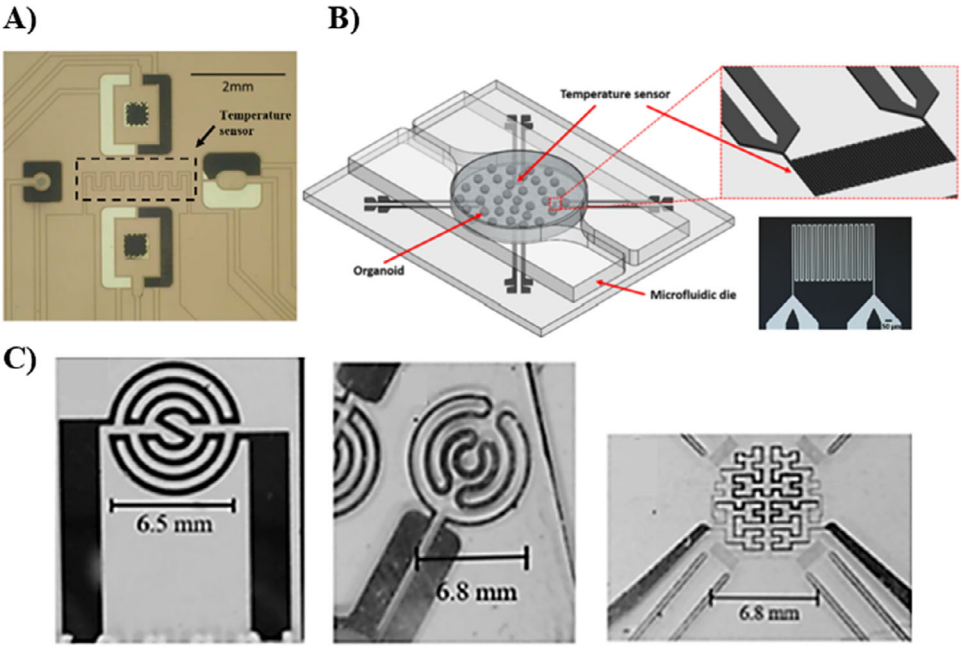

Figure 12. A) Photograph of a microfabricated screen-printed microbiosensor showing the temperature sensor developed by Pemberton et al.[67] Reproduced from[67] with permission from MDPI, under a Creative Commons Attribution (CC BY) license. Copyright 2014, MDPI. B) Schematic representation of the temperature sensors integrated in the organ-on-a-chip, fabricated by Sousa et al.[25] Reproduced from[25] with permission from MDPI, under a Creative Commons Attribution (CC BY) license. Copyright 2021, MDPI. C) Photographs of three configurations of aluminium microheaters.[100] Reproduced from[100] with permission from ELSEVIER, under a Creative Commons Attribution (CC BY) license. Copyright 2023, ELSEVIER.

integration of the OoC chamber with CMOS electronics, capable of controlling the microheater and featuring other relevant sensors and electronics into the same die.[101] Besides custom-made platinum and aluminium sensors, commercial temperature sensors have also been integrated into OoC devices. For instance, a type T (or Copper-Constantan) thermocouple wire with a diameter of 0.025″, working in the range between 0 and 150 °C and with a response time of 0.1 s was integrated by Zhang et al. in a modular platform, working in an automated manner for at least 5 days.[38] Taking advantage of a compact, low cost and miniaturized design, Ponte et al.[102] projected a smart temperature sensor on a modular silicon-based OoC device, using CMOS technology.[102] The authors used a system of two main blocks: a proportional to absolute temperature (PTAT) current generator (employing NPN bipolar transistors to sense the temperature information) and a relaxation oscillator. The authors obtained a sensor with 57.1 ns $°C^{-1}$ of sensitivity in a range of 20–100 °C.[102]

When comparing the main approaches for resistive temperature sensing in OoC systems, platinum-based sensors remain the benchmark in terms of accuracy, stability, and biocompatibility. Their excellent linearity and resistance to corrosion make them particularly suited for long-term operation in physiological environments. Thermocouples, although robust and fast-responding, are more difficult to miniaturize and integrate seamlessly within microfluidic architectures. Regarding actuators, aluminium-based heaters provide uniform heat distribution and are easier to pattern, but their lower stability and reduced resistance to oxidation can affect reproducibility over time. CMOS-based temperature sensors represent a newer and promising direction, allowing direct integration with other sensing and control elements on the same chip. While they generally offer lower precision than platinum sensors, their scalability, compactness, and compatibility with electronic readout circuits make them ideal for multiparametric and autonomous OoC platforms.

4. Integration and Fabrication Techniques

The use of new biomaterials[103] and advanced fabrication techniques[8] enabling novel layouts can accelerate and simplify OoC production, making these platforms increasingly physiologically relevant for biomedical studies.

Different sensing transduction principles inherently require distinct fabrication and integration strategies (**Table 5**), which direct impact device performance, reproducibility, and scalability. In OoC systems, optical, electrochemical, mechanical, and resistive transducers not only differ in their detection physics but also in how they are implemented within microfluidic architectures (Table 5).

4.1. Optical Transducers

The integration of optical sensors into OoC platforms poses several specific challenges, including the requirement for transparent substrates, accurate optical alignment, and adequate protection of luminescent dyes against photobleaching or leaching. These aspects directly impact the stability, reproducibility, and sensitivity of measurements.

Two main strategies are commonly adopted for optical sensing. The first involves soluble indicators (e.g., phenol red or luminescent dyes), which can be either dissolved in the culture

Table 5. Summary of integration and fabrication techniques of transduction systems, highlighting fabrication methods, strengths, and limitations.

Transduction	Fabrication / Integration Approaches	Strengths	Limitations
Optical	• Soluble dyes dispersed in medium or immobilized in thin films/membranes; Integrated photodiodes via CMOS; • Bonding with UV adhesives or plasma; PDMS (soft lithography) or PMMA (embossing, laser ablation, micromilling).	• Non-invasive • High sensitivity • Compatible with transparent substrates	• Requires optical transparency and alignment • Photobleaching • Dye leaching • Complex alignment • Limited scalability
Electrochemical	• Electrode deposition and patterning (sputtering, evaporation, printing) on glass, silicon, or polymers; passivation by PECVD/CVD (SiO_2, Si_3N_4, parylene-C); • Integration by adhesives, tapes, plasma, or thermal bonding.	• Wide analyte range • Multiplexing potential • High specificity and sensitivity	• Reference degradation • Insulation requirements • Sensitive to fouling and delamination • Complex calibration • Possible drift in long-term use
Mechanical	• Microfabrication of flexible membranes (soft lithography, 3D printing, electrospinning, solution casting); • Strain gauges by sputtering/printing metals or inks; • MEMS-based silicon or polymer pressure sensors; • Precise bonding to prevent leakage.	• Real-time mechanical information • Barrier and strain monitoring • Mimics physiological mechanics	• Material constraints • Complex alignment • Harder integration • Calibration needs
Resistive	• Patterning of conductive tracks (sputtering, evaporation, photolithography, or screen/inkjet printing) on rigid or flexible substrates (PDMS, thermoplastics); • Post-deposition annealing; • Use of adhesion/barrier layers.	• Simple architecture • Low-cost • Scalable • Good temperature and strain sensitivity • Suitable for flexible devices	• Limited multiplexing • Insulation requirements • Requires annealing control • Sensitive to thermal stress, diffusion and adhesion failures

medium or introduced as dispersed microbeads (**Figure 13 i**). This approach avoids complex fabrication steps, it is simple and fast to implement, making it useful for proof-of-concept studies or flexible experimental setups. However, since the sensing elements are not fixed, signal fluctuations can occur due to dye diffusion or degradation, and the presence of particles may interfere with cell behavior, ultimately reducing measurement stability over time.

The second strategy involves immobilizing the sensing material in a predefined location within the device, typically in the form of a thin film, membrane, or localized spot (Figure 13 ii). This method is often used for oxygen measurements, where luminescent dyes are embedded in a polymer matrix or coated onto channel walls. Immobilization ensures spatially defined sensing, improved stability, and enables repeated or continuous measurements in the same region. However, it requires additional processing steps, such as surface functionalization, immobilization chemistry, and calibration procedures, and may limit flexibility when multiple sensing points are needed and are prone to biofouling.

Therefore, for the optical transducers, the selection of an appropriate bonding method is highly dependent on the sensor die and matrix, making general recommendations challenging. However, non-thermal and solvent-free bonding techniques are preferred to preserve sensor stability. While UV-curable adhesives can be used, prolonged UV exposure should be avoided due to the degradation of the adhesive and surface damage.[10] Plasma bonding may alter sensor properties due to changes in the matrix surface; however, it has been successfully employed for bonding microfluidic chips with integrated luminescent sensors.[10,104]

Material selection also plays a key role in the successful integration of optical sensors. A large fraction of OoC devices is fabricated from PDMS due to its optical transparency, gas permeability, and ease of fabrication specially for prototyping. Furthermore, it presents interesting properties for biomedical applications, including physiological indifference, excellent resistance to biodegradation, biocompatibility, and chemical stability.[105]

Alternatively, PMMA and other thermoplastics offer higher mechanical stability, lower gas permeability, and improved dimensional control. They are typically processed through hot embossing, laser ablation, or micromilling. However, these materials require higher processing temperatures and more demanding bonding techniques compared to PDMS. PDMS can be directly cast and cured on top of rigid inorganic substrates, allowing conformal contact and seamless integration without the need for adhesives. In contrast, PMMA typically requires additional bonding processes, such as bonding, gluing, thermal, or solvent-assisted assembly, which are less flexible and more complex. Consequently, PMMA-based systems are generally less compatible with monolithic integration approaches.

A more advanced route involves CMOS-based technologies, which enable direct integration of optical detectors and electronic components onto silicon wafers. CMOS fabrication involves multiple steps, including photolithography, doping, metal deposition, and dielectric passivation. This allows embedding photodiodes, amplifiers, and signal processing circuitry directly on the

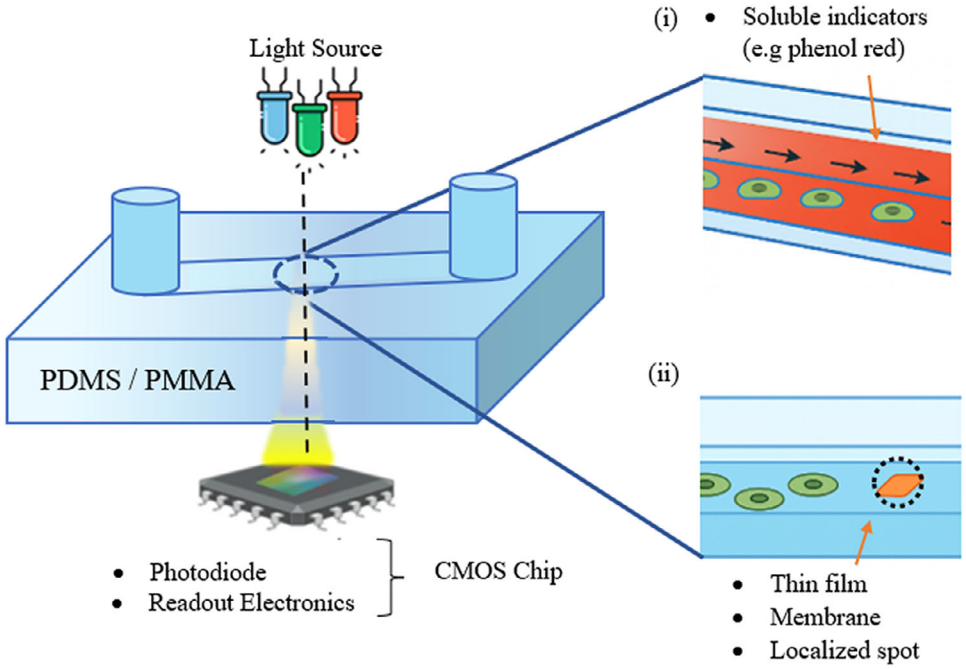

Figure 13. Schematic illustration of optical sensing integration in PDMS or PMMA-based microfluidic devices. Two main configurations are shown: i) soluble indicators, such as phenol red, dispersed within the flowing medium, and ii) immobilized sensing elements (thin films, membranes, or localized spots) integrated into the channel walls. The transmitted or emitted light is detected by a photodiode integrated with CMOS readout electronics, enabling real-time optical monitoring of the biological microenvironment.

chip, leading to compact systems with improved signal stability. The main limitations are the need for cleanroom facilities, lower flexibility for rapid prototyping, and more complex packaging to interface with the biological microenvironment.

4.2. Electrochemical Transducers

Electrochemical transducers rely on the deposition and patterning of conductive materials, often on glass, silicon, or thermoplastic substrates. These methods allow fine pattern control and reproducibility, but demand robust insulation and packaging to avoid electrode degradation in aqueous conditions (**Figure 14**).

Their performance depends on electrode material, fabrication method, and surface functionalization. Commonly used materials include platinum, gold, carbon-based materials, and conductive polymers like PEDOT:PSS. The standard used reference electrode is of Ag/AgCl, often formed by silver electrodeposition and chlorination.[74] Fabrication approaches vary in complexity. Whereas thin-film microfabrication (as metal sputtering and photolithography processes) enables precise and reproducible structures on glass or silicon,[74] printing techniques, such as screen or inkjet printing, offer a low-cost alternative and large availability in regular laboratories for rapid prototyping,[67,106] albeit with larger features sizes.

Passivation of electrochemical electrodes is critical to ensure electrical insulation, chemical stability, and reproducibility in OoC devices. The choice of method depends on the substrate, integration strategy, and desired performance. Thin-film techniques, such as chemical vapor deposition (CVD), physical vapor deposition (PVD), and evaporation, are commonly used to deposit uniform dielectric layers (e.g., SiO_2, Si_3N_4, Al_2O_3, parylene-C), providing chemical resistance and CMOS compatibility.[74] Parylene-C, in particular, offers conformal, biocompatible protection suitable for long-term applications and complex 3D structures.[107,108] Additionally, photopatternable materials, such as SU-8 or polyimide photoresists, can be spin-coated and UV-patterned to form thick, stable passivation layers that also serve structural functions, offering flexibility and chemical resistance.[109]

Other polymeric layers can also serve as passivation materials. For instance, PDMS coatings can be used both as protective layers and gas-permeable membranes, although their long-term stability is limited they offer simpler electrical insulation solutions at lower cost.

Other less common but valuable strategies include sol–gel coatings, which provide good chemical resistance and can be applied by dip or spray coating, and atomic layer deposition (ALD), which allows highly controlled but ultrathin films of materials.[110,111,112]

Electrochemical transducers are integrated into microfluidic and organ-on-a-chip platforms through several bonding approaches, each selected according to the materials and fabrication constraints of the device[113] (Figure 14). Liquid adhesives are often used as bonding agents, providing a straightforward and low-temperature method to seal sensor substrates to microfluidic layers while maintaining biocompatibility and avoiding damage to sensitive components. Alternatively, adhesive tapes offer a fast and reversible strategy for assembling multilayer structures, allowing easy alignment and replacement of individual

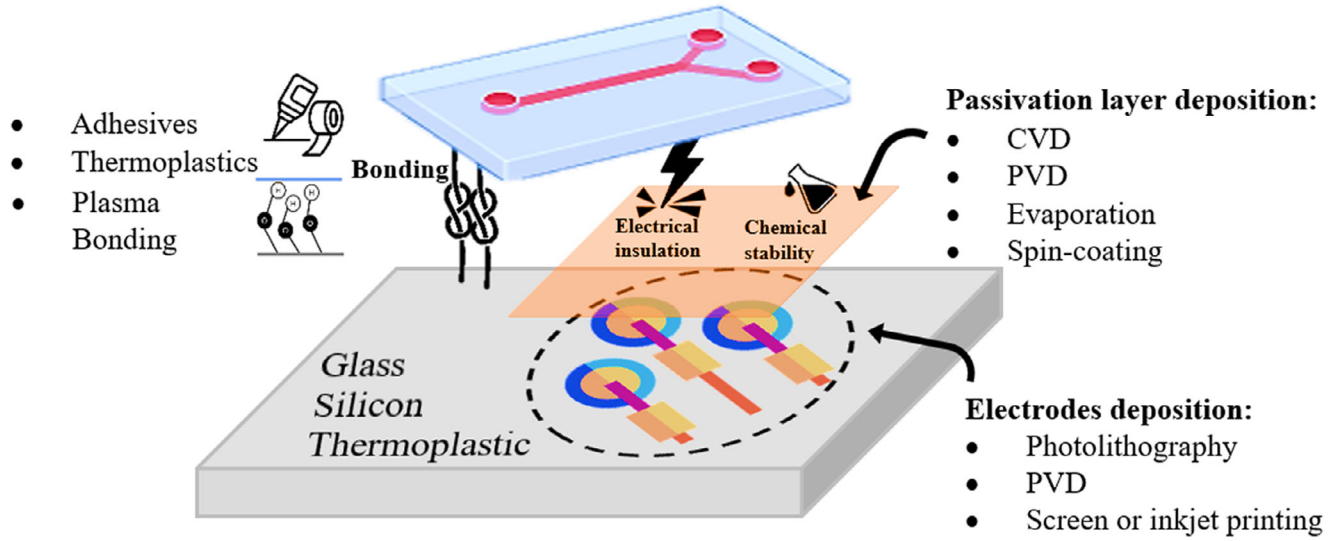

Figure 14. Schematic illustration of the fabrication and integration workflow for electrochemical sensors in OoC devices. The process involves the deposition of metallic electrodes on different substrates (glass, silicon, or thermoplastics) using photolithography, physical vapor deposition, or printing techniques. A passivation layer is subsequently deposited by CVD or PVD to ensure electrical insulation and chemical stability. The microfluidic module is bonded to the substrate via adhesives, thermoplastics, or plasma bonding to achieve full device integration.

components. Plasma bonding, which is particularly suited for PDMS-based microfluidic systems, enables the formation of strong covalent bonds between polymer surfaces, ensuring excellent sealing and optical transparency. In thermoplastic devices, thermal bonding using polymer foils is another effective technique, allowing the stable integration of electrodes and microchannels without the need for additional adhesives. More recently, multilayer nanotube membranes have been introduced as functional interlayers for sensor integration, improving both adhesion and the electrochemical performance of the embedded transducers.[113]

4.3. Mechanical Transducers

The fabrication of mechanical transducers in OoC platforms typically depends on the sensing principle, but most approaches are compatible with microfluidic integration.

For TEER-based systems, electrodes are usually patterned using photolithography or screen printing of conductive materials such as gold, platinum, or ITO on glass, thermoplastic substrates, or PDMS membranes (**Figure 15**). These electrodes can be integrated directly into the chip during fabrication or added as modular inserts bonded to the device.[114]

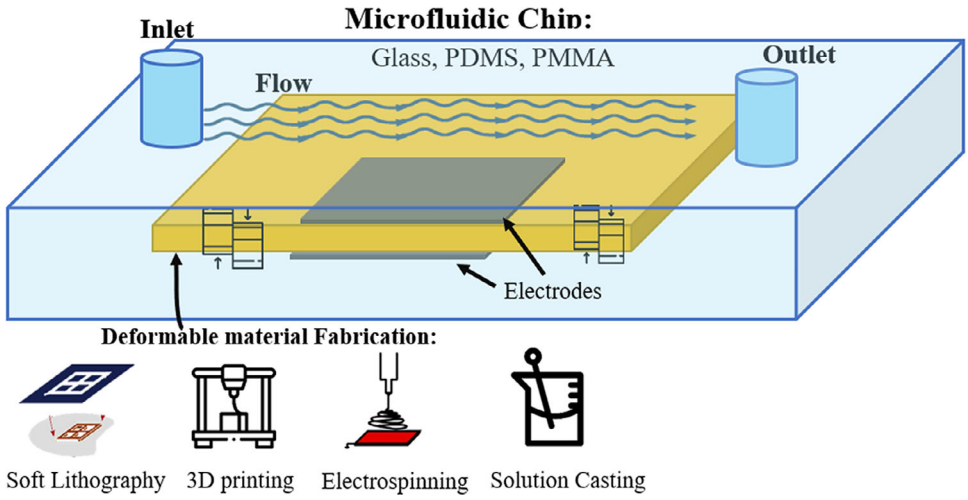

Figure 15. Schematic representation of the integration of deformable mechanical transducers within microfluidic and OoC systems. The device consists of a microfluidic chip (glass, PDMS, or PMMA) containing a deformable membrane positioned between microchannels. The membrane deflection can be actuated or sensed via embedded electrodes placed below or around the deformable material. Various fabrication techniques—such as soft lithography, 3D printing, electrospinning, and solution casting—are employed to produce flexible and biocompatible membranes with controlled mechanical properties suitable for simulating physiological motion and stress conditions.

For strain and deformation sensing, flexible membranes are first produced using soft lithography, 3D printing, electrospinning and solution casting[115] (Figure 15). Strain gauges are then formed by depositing and patterning thin metallic films or conductive inks, typically using sputtering, evaporation, or printing. These membranes are bonded to the microfluidic structure to allow real-time monitoring of tissue deformation.[116]

Pressure sensors are often fabricated using micro electro mechanical systems (MEMS), involving microstructuring of silicon or polymer substrates using lithography, etching, lift-off,[117] embossing,[118] or molding.[119,115] The sensing elements are then aligned and sealed with the microfluidic chip, frequently requiring precise bonding to avoid leakage and ensure stable signal transmission.

Integration strategies vary from simple modular electrode insertion to fully embedded MEMS devices. Modular systems are easier to fabricate and replace, while integrated sensors offer higher reproducibility, compactness, and potential for multiplexing but more complex fabrication. Proper alignment and bonding are critical to minimize signal drift and mechanical instability.

4.4. Resistive Transducers

The resistive transducers are structurally simple and relatively easy to integrate compared with other sensing modalities. Typical fabrication involves the patterning of thin conductive films or printed conductive tracks on rigid or flexible substrates. For high-resolution structures, metal sputtering or evaporation combined with photolithography and etching is frequently used to define platinum, aluminium, gold, silver, or doped semiconductor resistors.[120] These processes allow accurate control of geometry and resistance values, which is particularly important for temperature and strain sensing applications. For flexible or disposable devices, screen printing and inkjet printing of carbon, silver, or hybrid conductive inks on PDMS or thermoplastic substrates offer a lower-cost and rapid alternative.[121]

A key fabrication challenge is the thermal treatment (annealing) often required after oxide deposition or passivation. Annealing can significantly modify the electrical properties of the metal layer already deposited-changing grain structure, resistivity, or adhesion. For example, platinum thin films can experience resistance drift due to grain growth or even delamination under high annealing temperatures if adhesion is poor or thermal stresses accumulate. Similarly, gold and silver may undergo diffusion into surrounding layers, particularly in the absence of a proper adhesion or barrier layer.[98] These effects can compromise sensor performance and reproducibility, making process sequencing and temperature control critical in the fabrication of reliable resistive elements.

Overall, resistive transducers combine fabrication simplicity with good sensitivity and integration flexibility. However, their performance strongly depends on careful control of fabrication parameters, especially when multiple deposition and annealing steps are involved. Proper selection of materials and process order is therefore essential to maintain stable and reproducible signals in OoC applications.

4.5. Modular and Monolithic Integration

In recent years, there has been a significant evolution in the integration of sensors into OoC platforms, particularly concerning the architecture of the systems and the degree of miniaturization (**Table 6**).

Initially, several approaches offered a modular integration, where different sensors and functional units were incorporated separately but assembled into a single, coordinated structure. A remarkable example of this philosophy is presented by Zhang et al.,[38] who developed a platform in which the organ models and the fluidics channels, integrated in independent PDMS devices, are connected by tubing, as well as the biosensing electrochemical module for biomarkers and the physical/chemical sensing module for pH, (O_2, and temperature monitorization all connected in a modular way (**Figure 16A**).[38] The authors claimed long-term monitor of the organ models parameters. However, the complete system required a high complex operation. Similarly, Huang et al.[122] also used a hybrid approach, combining a PDMS microfluidic module with PMMA microwells, onto which an O_2-sensitive layer was deposited, followed by a pH-sensitive layer, forming a dual luminescent sensor. The reading system was composed of LEDs, optical fibers, and commercial photodiodes. On the other hand, Müller et al.[45] 3D printed microfluidic chips in thermoplastic cyclic olefin copolymer (COC) and deposited optical indicators using a microdispenser MDS3200+ (VERMES Microdispensing GmbH), maintaining the principle of separate functional modulation, with optical fibers and photodiodes (Figure 16B). Shah et al.[123] followed a similar modular strategy, integrating an optical O_2 sensor (commercial optode) and a TEER sensor using STX2 electrodes between two polycarbonate (PC) enclosures, that compress silicone rubber gaskets to form spiral-shaped microchambers (Figure 16C).[123] The bonding of the PC membrane to the microchamber was performed by medical-grade double-sided adhesive tape. In contrast, Asif et al.[124] developed a compact hybrid system combining a silicon elastomer-based microfluidic chip fabricated in a 3D printer, with an optical pH sensor and a TEER sensor. The pH sensor used a white LED, an optical fiber, and a photodiode integrated into a custom transparent tube, while TEER was measured via ITO electrodes screen-printed onto a glass substrate.[124]

Despite the versatility and ease of maintenance offered by the modular approach, especially in the context of prototyping and experimentation, there is a clear trend toward total functional integration into a single platform or chip, monolithic integration, particularly driven by objectives such as miniaturization, portability, automation, ease of production, and industrial scalability. In this regard, the works of Pemberton et al.,[67] Dornhof et al.,[68] Krommenhoek et al.,[72] Khalid et al.[125] and Curto et al.[126] represent an important turning point. Pemberton et al.[67] developed a fully integrated system for cell biomarkers on a silicon substrate, with electrochemical pH (based on IrOx), O_2, glucose, and lactate sensors (**Figure 17A**). The IrOx was deposited by reactive sputtering, and all platinum tracks and electrodes were fabricated by optical lithography and dry etching processes. In addition, platinum-based temperature sensors were embedded under a SiO_2/Si_3N_4 layer, all within five functional wells. The SiO_2/Si_3N_4 layers were deposited by plasma-enhanced chemical vapor deposition (PECVD), and patterned using lithography and

Table 6. Comparative analysis of OoC modular and monolithic integrated platforms.

Refs.	Methods and analytes	Substrate and microchannels	Transducers and materials	Main function	Integration
[38]	Optical (pH, O_2) Resistive (Temperature) Electrochemical (GST-α, CK-MB)	PDMS microchannel	LEDS and Si photodiodes Thermocouple Probe Au electrodes	Studying drug-induced organ toxicity in cancer heart and liver models.	Modular
[122]	Optical (pH, O_2)	PMMA substrate, glass lid and PDMS microposts	LEDS, photo-multiplier tube and CCD camera	Examination of the respiration and embryonic acid extrusion of a single developing zebrafish embryo	
[45]	Optical (pH, O_2)	Thermoplastic COC microfluidic chip	Optical Fibers and sensors	Monitoring the metabolic response of a human lung carcinoma epithelial-like cell line	
[123]	Optical (O_2) Electrochemical (Cell growth and differentiation)	Polycarbonate enclosures and Silicone rubber gaskets	TEER electrodes Optodes and fiber optics	Co-culture of human and microbial cells under conditions representative of the gastrointestinal human–microbe interface	
[124]	Optical (pH) TEER (monitor the epithelial barrier function)	Glass based chip with silicone gel for channel printing	OECT Gold electrodes	Live monitoring of cellular growth pattern for a theranostic proximal tubule-on-a-chip model	
[67]	Electrochemical (pH, O_2, Glucose and lactate) Resistive (Temperature)	Si substrate and SiO_2 Pt temperature sensor	IrOx pH sensor Pt O_2, glucose and lactate sensors	Monitoring cell metabolic activity, including toxicity testing of candidate drugs in the pharmaceutical industry	Monolithic
[68]	Electrochemical (O_2, Glucose and lactate)	Glass chip	Platinum electrodes	Matrix-based organoid cultivation	
[72]	Electrochemical (Biomass, O_2, pH) Resistive (Temperature)	Oxidized silicon substrate ISFET pH sensor	Pt for O_2, biomass and temperature sensors	On-line monitoring of fermentor conditions in both miniaturized cell assays and in industrial scale fermentations	
[125]	Electrochemical (O_2 and reactive oxygen species)	Glass chip with Silicon elastomer microfluidic channels PMMA layer cover	Au and Ag electrodes	Monitoring developmental (initially normoxia) and induced hypoxia in a custom-developed gut bilayer microfluidic chip platform	
[126]	Electrochemical (Glucose) TEER (Barrier tissue integrity)	Glass substrate PMMA channel	OECT Gold electrodes	Multiple different methods for assessing cell morphology, differentiation, and integrity	

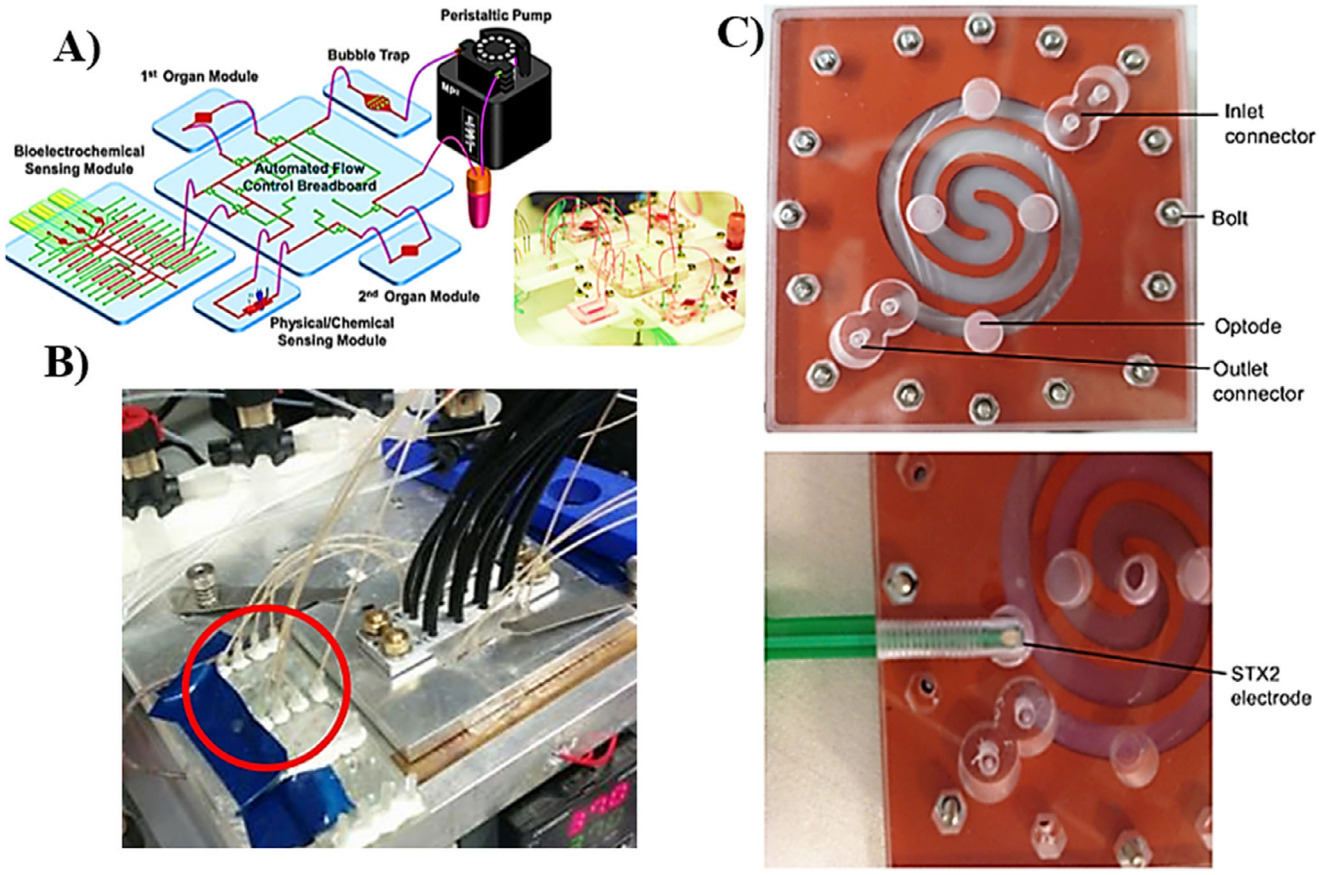

Figure 16. A) Schematic of the integrated microfluidic device developed by Zhang et al.,[38] consisting of modular components including microbioreactors, breadboard, reservoir, bubble trap, physical sensors, and electrochemical biosensors.[38] Reproduced from[38] with permission of National Academy of Sciences. Copyright 2017, National Academy of Sciences. B) Physical design parameters of the HuMiX device developed by Shah et al.[123] Reproduced from[123] with permission of Springer nature. Copyright 2016, Springer nature. C) Chip holder with the optic block by Müller et al.,[45,122] Reproduced from[45] with permission from ELSEVIER, under a Creative Commons Attribution (CC BY) license. Copyright 2021, ELSEVIER.

reactive ion etching in a CHF_3/O_2 mixture to leave exposed platinum pads. Dornhof et al.[68] followed a similar approach, integrating O_2, glucose, and lactate sensors on a glass wafer insulated with a Si_3N_4 layer (Figure 17B). The microchannels were fabricated by photolithography using permanent epoxy photoresist (SU-8) and a Poly(methyl methacrylate) (PMMA) covering to the fluidic unit.[70] The integrated platform was tested for monitoring and quantifying multi-analyte metabolite comsumption during one week. Electrical connection was made via printed circuit board (PCB) bonded with epoxy adhesive.[68] Krommenhoek et al.[72] used ISFETs with Ta_2O_5 gates for pH monitorization, and a platinum electrode for O_2 and biomass monitoring, also integrating resistive temperature and heating transducers directly on an oxidized silicon substrate, for an online monitoring of relevant fermentor conditions.[72] The ISFETs with Ta_2O_5 gates were fabricated using standard photolithography to define doped drain and source regions. Tantalum was deposited and oxidized to form the sensing gate, with aluminum sputtered for electrical contacts and platinum for the remaining metal structures, using tantalum as an adhesion layer. A lift-off process was employed to avoid damage from wet etching, and non-sensitive areas were passivated with a photopatterned polyimide layer.[72] Khalid et al.[125] explored the integration of O_2 and reactive oxygen species (ROS) sensors on glass, with gold and silver electrodes printed by a dispenser system, and microfluidic channels also printed with medical-grade elastomer, forming a multilayer architecture supported by PMMA and a porous polycarbonate membrane for bilayer cultures (Figure 17C). Finally, Curto et al.[126] proposed a platform based on organic transistors (PEDOT:PSS) with gold transistors channels and gate electrodes, integrating glucose and TEER sensors, with microfluidics coupled by PSA adhesive and silicone rubber inlet ports. The transistor channels and gate were patterned using a parylene C (PaC), while the active layer of the transistor channel and the gate electrode were performed using PEDOT:PSS.[126] PEDOT:PSS is a conducting polymer commonly employed as the active layer of OECTs, due to its easy processability, chemical tunability, and biocompatibility.[126] Curto et al.[126] made a significant breakthrough in coupling OECTs with microfluidics, achieving a multi-parametric transducer platform.

Comparing the two approaches (Table 6), i.e., modular systems and monolithic modules where everything is produced into a single substrate, it is clear that, despite simpler to configure and modify, modular systems have limitations in terms of

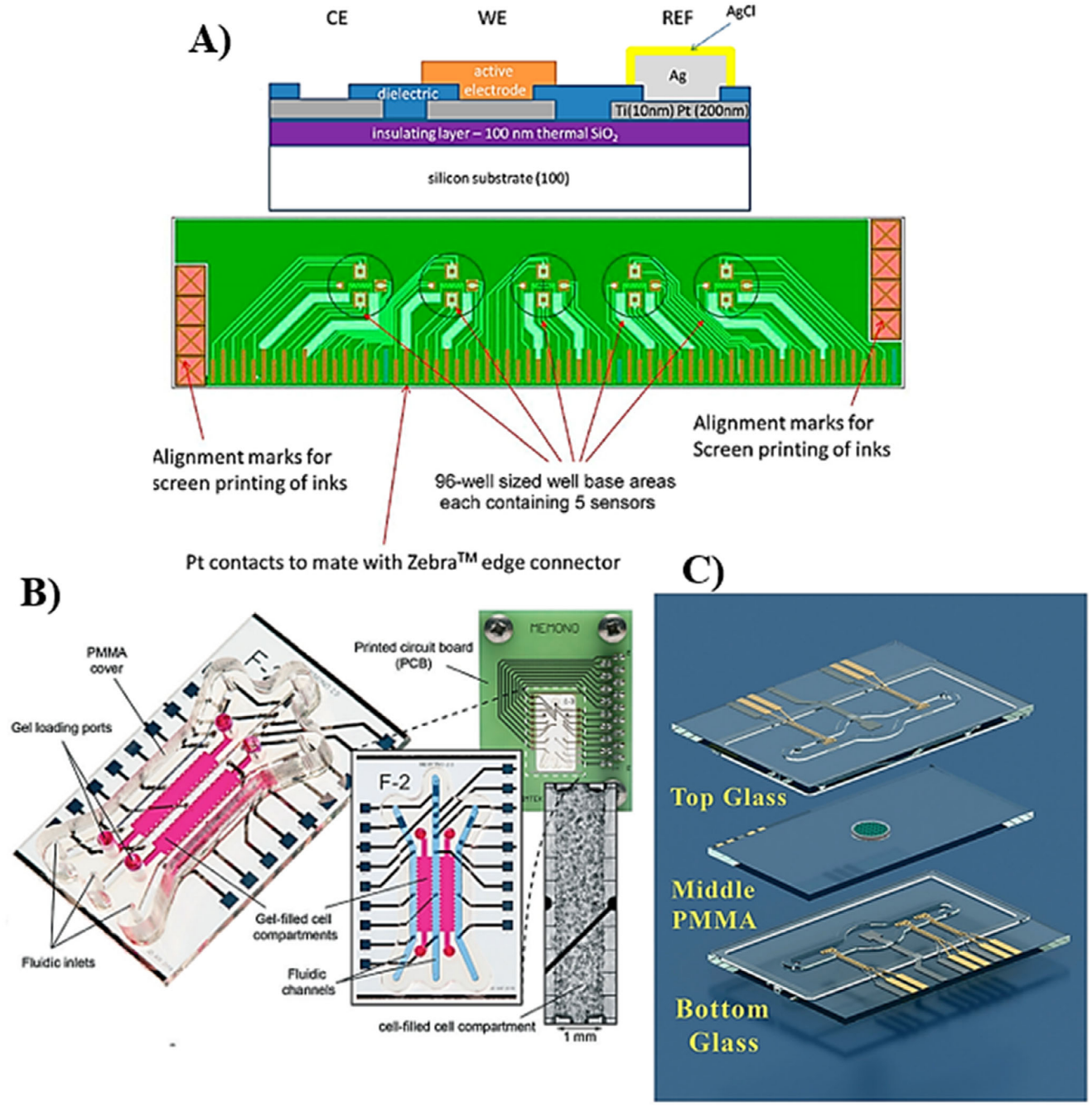

Figure 17. A) Diagram illustrating cross-section (not to scale) through the MEMS-microfabricated sensor device platform. Overall view of the design for the 5-well MEMS sensor chip with five sensors per well base (25 sensors in total). Bottomless wells have been added to the surface of the MEMS chips.[67] Reproduced from[67] with permission from MDPI, under a Creative Commons Attribution (CC BY) license. Copyright 2014, MDPI. B) Photographs of an assembled device filled with colored hydrogel and with attached PMMA-cover. Electrical sensor readout is done by means of a custom-made printed circuit board. Phase-contrast micrograph shows breast cancer stem cell (BCSC1) spheroids within a spheroid compartment after five days of culture.[68] Reproduced from[68,67] with permission from Royal Society of Chemistry, under a Creative Commons Attribution (CC BY) license. Copyright 2022, Royal Society of Chemistry. C) Annotated expanded view of the bilayer microfluidic chip.[125] Reproduced from[125,68,67] with permission from Royal Society of Chemistry. Copyright 2022, Royal Society of Chemistry.

miniaturization and automation, and are heavily reliant on commercial optical components (LEDs, fibers, photodiodes). On the other hand, fully integrated systems on silicon or glass substrates are more compact, reproducible, and compatible with large-scale industrial processes. Furthermore, these miniaturized systems offer lower volume, reduced energy consumption, and greater potential for portable, implantable, or point-of-care applications.[127] This represents a paradigmatic shift in bioanalytical device engineering, bringing organ-on-a-chip platforms closer to full functional integration at the micro/nanometric scale.

5. Challenges and Future Directions

Despite the advances in modular sensor integration within organ-on-a-chip platforms, recent studies reported in the literature show a growing trend toward replacing optical sensors with electrochemical ones, particularly in systems featuring full integration within a monolithic module. This shift is largely driven by the relative ease of integrating and fabricating of electrochemical (bio)sensors in microenvironments, especially when using substrates like glass or silicon and standard clean room processes. However, this approach often sacrifices the high sensitivity and selectivity typically offered by optical sensors, as well as their potential for flexibility, multiplexing, non-invasive, real-time, and mainly long-term monitoring. Additionally, in a multi-OoC platform, it is also required the analysis of the effect of cellular responses and microenvironmental changes due to inter-organs communication, which requires a continuously measurement strategy, specially tailored for optical methods, where fouling and degradation electrodes are not applied. An emerging solution to overcome the more complex integration of optical transducers is the application of CMOS technology, which enables the monolithic integration of light sources, photodetectors, and readout circuitry. Moreover, for the development of an organ-on-a-chip platform capable of simultaneously monitor multiple parameters, such as temperature, pH, oxygen, glucose, lactase, among others, and enabling a monolithic configuration, silicon stands out as a highly versatile and suitable material to serve as the substrate.[128] Its compatibility with cleanroom microfabrication techniques (wet etching, plasma etching, laser processing, and bonding methods)[128] as well as the possibility of integration with aluminium or platinum-based transducers, photodetectors, and integrated circuits in CMOS, makes it particularly advantageous for the creation of miniaturized and multiparametric device. This paves the way for highly miniaturized optical sensors that are fully compatible with microfluidic environments and can be seamlessly integrated with readout electronics.[129] Such convergence promises to combine the best of both worlds: the practicality of microfabrication with the advanced performance of optical detection. Moreover, the fast evolution of photonics integrated circuits will lead to new optical sensors approaches that not rely only in endpoint measurements but also will be able to assess cellular response with a 3D spatial resolution. This could be a breakthrough in multimodal sensing for continuously physiological events measurements in multi-OoC devices.

Looking even forward, future OoC sensing modalities are expected to combine multi-physics transduction principles, leveraging optical, electrochemical, and mechanical responses within the same platform. This hybridization will improve data robustness and reduce cross-sensitivity among parameters, allowing inter-organ interactions, which could have a transformative path in precision medicines.[130] Moreover, nanostructured materials, 2D semiconductors, and organic transistors (such as OECTs) are emerging as promising alternatives for biocompatible, low-power, and flexible sensing layers.[131,132] These materials offer tunable electrical properties and mechanical flexibility compatible with polymeric substrates, enabling direct integration with soft microfluidic architectures. Despite their potential, challenges such as long-term stability, device encapsulation, and reproducibility remain to be addressed before large-scale implementation in organ-on-a-chip systems.

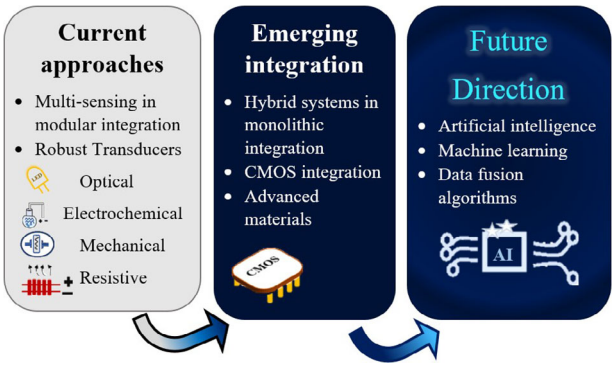

Figure 18. Schematic summary of the main current and future challenges to be addressed for transducers' integration in OoC devices.

Finally, the incorporation of artificial intelligence (AI),[133] machine learning (ML),[134] and data fusion algorithms is set to redefine the landscape of OoC analysis. By integrating multiple sensor outputs into unified predictive models, these AI-enhanced systems can rapidly and autonomously extract hidden correlations, identify early signs of toxicity, and provide feedback for optimizing experimental design in real time. This new paradigm will transform OoCs from traditional, passive, and resource-intensive analytical tools into active, intelligent platforms capable of providing dynamic biological insights, ultimately positioning them as a gold standard in personalized medicine. Despite this potential, challenges remain: the large and heterogeneous datasets produced by high-throughput OoCs require standardization, careful preprocessing, and high-quality annotations for robust ML training. Integrating multimodal data from imaging, sensors, and fluidics is technically complex, and the "black-box" nature of many AI models raises concerns about interpretability, reproducibility, and regulatory acceptance. Addressing these issues through explainable AI, standardized datasets, interoperable formats, and closed-loop automation will be key for realizing adaptive OoCs as gold-standard platforms for drug development, toxicity testing, and patient-specific therapeutic screening.

In summary, the future of OoC technologies lies at the intersection of advanced materials,[135] integrated microfabrication, and data-driven analytics, as summarized in **Figure 18**. The synergistic development of these areas will enable the next-generation of OoC platforms that are fully autonomous, scalable, and capable of reproducing human physiology with unprecedented precision.

6. Conclusion

This review has provided a comprehensive exploration of transducers for monitoring and controlling physicochemical and environmental parameters, particularly pH, oxygen, glucose, lactate, and temperature, to maintain viable cellular organ models in OoC platforms. Optical-based technologies show promising advances due to their flexibility, multiplexing, non-invasiveness, and ability for real-time, continuous, and long-term monitoring. However, challenges related to microfabrication need to be addressed. Temperature and mechanical transduction are crucial for heating, dynamic stimuli, and flow conditions setting a physiologically relevant environment.

Therefore, future research should focus on developing hybrid transducing systems integrated into a single advanced OoC platform for real-time monitoring. Additionally, employing sensor data fusion and machine learning techniques can provide insights into transducers interaction, expand the range of measurable parameters, and enhance data processing and decision-making capabilities. Addressing these challenges could support a true transformative potential for driving the clinical translation of OoC platforms in personalized therapy.

Acknowledgements

This work was supported by the project PTDC/EEI-EEE/2846/2021 (https://doi.org/10.54499/PTDC/EEI-EEE/2846/2021), through national funds (OE), within the scope of the Scientific Research and Technological Development Projects (IC&DT) program in all scientific domains (PTDC), through the Foundation for Science and Technology, I.P. (FCT, I.P). The authors also acknowledge the partial financial support within the R&D Unit Project Scope: UID/4436/2025, LA/P/0029/2020.

Open access publication funding provided by FCT (b-on).

Conflict of Interest

The authors declare no conflict of interest.

Keywords

integration, microfabrication, organ-on-a-chip, transducers

Received: August 26, 2025
Revised: November 13, 2025
Published online: December 17, 2025

[1] A. E. Danku, E. H. Dulf, C. Braicu, A. Jurj, I. Berindan-Neagoe, *Front. Bioeng. Biotechnol.* **2022**, *10*, 840674.
[2] J. F. Feitor, L. C. Brazaca, A. M. Lima, V. G. Ferreira, G. Kassab, V. S. Bagnato, E. Carrilho, D. R. Cardoso, *ACS Biomater. Sci. Eng.* **2022**, *9*, 2220
[3] W. Sun, Y.-Q. Chen, G.-A. Luo, M. Zhang, H.-Y. Zhang, Y.-R. Wang, P. Hu, *Chinese J. Anal. Chem.* **2016**, *44*, 533.
[4] G. A. Clarke, B. X. Hartse, A. E. Niaraki Asli, M. Taghavimehr, N. Hashemi, M. Abbasi Shirsavar, R. Montazami, N. Alimoradi, V. Nasirian, L. J. Ouedraogo, N. N. Hashemi, *Sensors* **2021**, *21*, 1367.
[5] S. Cho, S. Lee, S. I. Ahn, *Eng. Lett.* **2023**, *13*, 97.
[6] J. Shi, L. Tong, W. Tong, H. Chen, M. Lan, X. Sun, Y. Zhu, *TrAC Trends Anal. Chem.* **2019**, *117*, 263.
[7] I. A. Morales, C.-M. Boghdady, B. E. Campbell, C. Moraes, *Front. Bioeng. Biotechnol.* **2022**, *10*, 11.
[8] V. Carvalho, I. Gonçalves, T. Lage, R. O. Rodrigues, G. Minas, S. F. C. F. Teixeira, A. S. Moita, T. Hori, H. Kaji, R. A. Lima, *Sensors* **2021**, *21*, 3304.
[9] S. Scott, Z. Ali, *Micromachines* **2021**, *12*, 319.
[10] S. Fuchs, S. Johansson, A. Ø. Tjell, G. Werr, T. Mayr, M. Tenje, *ACS Biomater. Sci. Eng.* **2021**, *7*, 2926.
[11] H. Chen, Z. Luo, X. Lin, Y. Zhu, Y. Zhao, *Nano Res.* **2023**, *16*, 10072.
[12] W. Yang, T. Li, S. Liao, J. Zhou, L. Huang, *TrAC Trends Anal. Chem.* **2024**, *172*, 117569.
[13] P. Tawade, M. Mastrangeli, *ChemBioChem* **2024**, *25*, 202300560.
[14] D. Kattipparambil Rajan, J. Verho, J. Kreutzer, H. Valimaki, H. Ihalainen, J. Lekkala, M. Patrikoski, S. Miettinen, in *2017 IEEE Int. Symp. Med. Meas. Appl.* , IEEE, New York NY USA **2017**, pp. 470-474.
[15] E. Tanumihardja, W. Olthuis, A. van den Berg, *Sensors* **2018**, *18*, 2901.
[16] R. I. Freshney, *Culture of Animal CellsCulture of Animal Cells*, Wiley, Hoboken NJ USA **2010**.
[17] E. B. Magnusson, S. Halldorsson, R. M. T. Fleming, K. Leosson, *Opt. Express* **2013**, *4*, 1749.
[18] I. M. Gonçalves, V. Carvalho, R. O. Rodrigues, D. Pinho, S. F. C. F. Teixeira, A. Moita, T. Hori, H. Kaji, R. Lima, G. Minas, *Cancers* **2022**, *14*, 935.
[19] M. Flinck, S. H. Kramer, S. F. Pedersen, *Acta Physiol.* **2018**, *223*, 13068.
[20] S. Munan, R. Yadav, N. Pareek, A. Samanta, *Analyst* **2023**, *148*, 4242.
[21] M. Azimzadeh, P. Khashayar, M. Amereh, N. Tasnim, M. Hoorfar, M. Akbari, M.-B. Oxygen, *Biosensors* **2021**, *12*, 6.
[22] P. E. Oomen, M. D. Skolimowski, E. Verpoorte, *Lab Chip* **2016**, *16*, 3394.
[23] J. W. Wilson, D. Shakir, M. Batie, M. Frost, S. Rocha, *FEBS J.* **2020**, *287*, 3888.
[24] T. Kilic, F. Navaee, F. Stradolini, P. Renaud, S. Carrara, *Microphysiological Syst.* **2018**, *1*, 1.
[25] P. J. Sousa, V. C. Pinto, V. H. Magalhães, R. O. Rodrigues, P. C. Sousa, G. Minas, *Appl. Sci.* **2021**, *11*, 3864.
[26] V. Srinivasan, V. K. Pamula, R. B. Fair, *Anal. Chim. Acta* **2004**, *507*, 145.
[27] J. Park, *Sensors* **2021**, *21*, 4474.
[28] S. Goldrick, K. Lee, C. Spencer, W. Holmes, M. Kuiper, R. Turner, S. S. Farid, *Biotechnol. J.* **2018**, *13*, 1700607.
[29] K. Torimoto, K. Okuno, R. Kuroda, N. Shanas, S. M. Cicalese, K. Eguchi, K. J. Elliott, T. Kawai, C. B. Corbett, A. M. Peluzzo, A. K. St Paul, M. V. Autieri, R. Scalia, V. Rizzo, T. Hashimoto, S. Eguchi, *Am. J. Physiol. Physiol.* **2022**, *322*, C73.
[30] X. T. Zheng, H. Bin Yang, C. M. Li, *Anal. Chem* **2010**, *82*, 5082.
[31] A. G. Correa-Mena, L. A. Gonzalez, L. J. Quintero-Rodriguez, I. E. Zaldivar-Huerta, in *2017 IEEE Mex. Humanit. Technol. Conf.*, IEEE, New York NY USA **2017**, pp. 170.
[32] M.-H. Wu, J.-L. Lin, J. Wang, Z. Cui, Z. Cui, *Biomed. Microdevices* **2009**, *11*, 265.
[33] M. A. U. Khalid, Y. S. Kim, M. Ali, B. G. Lee, Y. J. Cho, K. H. Choi, *Biochem. Eng. J.* **2020**, *155*, 107469.
[34] H. M. U. Farooqi, M. A. U. Khalid, K. H. Kim, S. R. Lee, K. H. Choi, *J. Micromechanics Microengineering* **2020**, *30*, 115013.
[35] E. N. Amran, S. Sudik, A. F. Omar, M. H. Mail, A. Seeni, *Photodiagnosis Photodyn. Ther.* **2019**, *27*, 380.
[36] A. Morgan, D. Babu, B. Reiz, R. Whittal, L. Y. K. Suh, A. G. Siraki, *Chem. Biol. Interact.* **2019**, *310*, 108739.
[37] S. A. M. Shaegh, F. De Ferrari, Y. S. Zhang, M. Nabavinia, N. B. Mohammad, J. Ryan, A. Pourmand, E. Laukaitis, R. B. Sadeghian, A. Nadhman, S. R. Shin, A. S. Nezhad, A. Khademhosseini, M. R. Dokmeci, *Biomicrofluidics* **2016**, *10*, 044111.

[38] Y. S. Zhang, J. Aleman, S. R. Shin, T. Kilic, D. Kim, S. A. M. Shaegh, S. Massa, R. Riahi, S. Chae, N. Hu, H. Avci, W. Zhang, A. Silvestri, A. S. Nezhad, A. Manbohi, F. De Ferrari, A. Polini, G. Calzone, N. Shaikh, P. Alerasool, E. Budina, J. Kang, N. Bhise, J. Ribas, A. Pourmand, A. Skardal, T. Shupe, C. E. Bishop, M. R. Dokmeci, A. Atala, et al., *Proc. Natl. Acad. Sci. USA* **2017**, *114*, E2293.
[39] A. A. Santos, G. M. Ferreira, P. J. Sousa, P. C. Sousa, S. O. Catarino, G. Minas, *Photonics* **2024**, *11*, 1130.
[40] H. K. Chandrasekharan, K. L. Wlodarczyk, W. N. MacPherson, M. M. Maroto-Valer, *Sci. Rep.* **2023**, *14*, 2839.
[41] M. Cao, S. K. Mahto, O. Yadid-Pecht, *IEEE Sens. J.* **2016**, *16*, 3611.
[42] A. V. Saetchnikov, E. A. Tcherniavskaia, V. A. Saetchnikov, A. Ostendorf, arXiv, **2024**, arXiv:2403.15117.
[43] D. Wencel, T. Abel, C. McDonagh, *Anal. Chem.* **2014**, *86*, 15.
[44] E. Saygili, U. Devamoglu, E. Bayir, O. Yesil-Celiktas, *J. Ind. Eng. Chem.* **2023**, *121*, 190.
[45] B. Müller, P. Sulzer, M. Walch, H. Zirath, T. Buryška, M. Rothbauer, P. Ertl, T. Mayr, *Sensors Actuators B Chem* **2021**, *334*, 129664.
[46] M. S. Moghaddam, H. Latifi, E. Abedini, M. Ghazanfar, E. Behroodi, M. S. Sadeghi, *IEEE Sens. J.* **2022**, *23*, 97.
[47] P. C. Thomas, M. Halter, A. Tona, S. R. Raghavan, A. L. Plant, S. P. Forry, *Anal. Chem.* **2009**, *81*, 9239.
[48] E. G. B. M. Bossink, J. V. M. Slob, D. Wasserberg, L. I. Segerink, M. Odijk, presented at 2020 IEEE *Sensors*, Rotterdam, Netherlands, October **2020**.
[49] S. Matsumoto, E. Leclerc, T. Maekawa, H. Kinoshita, M. Shinohara, K. Komori, Y. Sakai, T. Fujii, *Sensors Actuators B Chem* **2018**, *273*, 1062.
[50] J. Ehgartner, P. Sulzer, T. Burger, A. Kasjanow, D. Bouwes, U. Krühne, I. Klimant, T. Mayr, *Sensors Actuators B Chem* **2016**, *228*, 748.
[51] H. Zirath, S. Spitz, D. Roth, T. Schellhorn, M. Rothbauer, B. Müller, M. Walch, J. Kaur, A. Wörle, Y. Kohl, T. Mayr, P. Ertl, *Lab Chip* **2021**, *21*, 4237.
[52] A. P. Vollmer, R. F. Probstein, R. Gilbert, T. Thorsen, *Lab Chip* **2005**, *5*, 1059.
[53] D. S. Daivasagaya, L. Yao, K. Y. Yung, M. Hajj-Hassan, M. C. Cheung, V. P. Chodavarapu, F. V. Bright, *Sensors Actuators B Chem* **2011**, *157*, 408.
[54] L. Shen, M. Ratterman, D. Klotzkin, I. Papautsky, *Sensors Actuators B Chem* **2011**, *155*, 430.
[55] S. Fuchs, V. Rieger, A. Ø. Tjell, S. Spitz, K. Brandauer, R. Schaller-Ammann, J. Feiel, P. Ertl, I. Klimant, T. Mayr, *Biosens. Bioelectron.* **2023**, *237*, 115491.
[56] E. Ryckeboer, R. Bockstaele, M. Vanslembrouck, R. Baets, *Opt. Express* **2014**, *5*, 1636.
[57] J. Kottmann, J. Rey, M. Sigrist, *Sensors* **2016**, *16*, 1663.
[58] I. Ahmed, N. Jiang, X. Shao, M. Elsherif, F. Alam, A. Salih, H. Butt, A. K. Yetisen, *Sensors & Diagnostics* **2022**, *1*, 1098.
[59] M. R. Kaysir, T. M. Zaman, S. Rassel, J. Wang, D. Ban, *Sensors* **2024**, *24*, 6963.
[60] M. Goodarzi, W. Saeys, *Talanta* **2016**, *146*, 155.
[61] K. Maruo, T. Oota, M. Tsurugi, T. Nakagawa, H. Arimoto, M. Hayakawa, M. Tamura, Y. Ozaki, Y. Yamada, *Appl. Spectrosc.* **2006**, *60*, 1423.
[62] S. Spitz, S. Schobesberger, K. Brandauer, P. Ertl, *Transl. Med.* **2024**, *9*, 10604.
[63] H. Takehara, O. Kazutaka, M. Haruta, T. Noda, K. Sasagawa, T. Tokuda, J. Ohta, *AIP Adv.* **2017**, *7*, 095213.
[64] R. Rizzo, V. Onesto, S. Forciniti, A. Chandra, S. Prasad, H. Iuele, F. Colella, G. Gigli, L. L. del Mercato, *Biosens. Bioelectron.* **2022**, *212*, 114401.
[65] F. A. R. Mota, M. L. C. Passos, J. L. M. Santos, M. L. M. F. S. Saraiva, *Biosens. Bioelectron.* **2024**, *251*, 116095.
[66] A. Weltin, K. Slotwinski, J. Kieninger, I. Moser, G. Jobst, M. Wego, R. Ehret, G. A. Urban, *Lab Chip* **2014**, *14*, 138.
[67] R. Pemberton, T. Cox, R. Tuffin, G. Drago, J. Griffiths, R. Pittson, G. Johnson, J. Xu, I. Sage, R. Davies, S. Jackson, G. Kenna, R. Luxton, J. Hart, *Sensors* **2014**, *14*, 20519.
[68] J. Dornhof, J. Kieninger, H. Muralidharan, J. Maurer, G. A. Urban, A. Weltin, *Lab Chip* **2022**, *22*, 225.
[69] Y. Mermoud, M. Felder, J. D. Stucki, A. O. Stucki, O. T. Guenat, *Sensors Actuators B Chem* **2018**, *255*, 3647.
[70] M. T. Ghoneim, A. Nguyen, N. Dereje, J. Huang, G. C. Moore, P. J. Murzynowski, C. Dagdeviren, *Chem. Rev.* **2019**, *119*, 5248.
[71] S. M. Bonk, M. Stubbe, S. M. Buehler, C. Tautorat, W. Baumann, E. D. Klinkenberg, J. Gimsa, *Biosensors* **2015**, *5*, 513.
[72] E. E. Krommenhoek, J. G. E. Gardeniers, J. G. Bomer, X. Li, M. Ottens, G. W. K. van Dedem, M. Van Leeuwen, W. M. van Gulik, L. A. M. van der Wielen, J. J. Heijnen, A. van den Berg, *Anal. Chem.* **2007**, *79*, 5567.
[73] H. Aydogmus, M. Hu, L. Ivancevic, J.-P. Frimat, A. M. J. M. van den Maagdenberg, P. M. Sarro, M. Mastrangeli, *Sci. Rep.* **2023**, *13*, 8062.
[74] F. Liebisch, A. Weltin, J. Marzioch, G. A. Urban, J. Kieninger, *Sensors Actuators B Chem* **2020**, *322*, 128652.
[75] A. Koklu, D. Ohayon, S. Wustoni, A. Hama, X. Chen, I. McCulloch, S. Inal, *Sensors Actuators B Chem* **2021**, *329*, 129251.
[76] Y. Wu, G. Wu, P. Fu, M. Hu, *E3S Web Conf* **2020**, *218*, 04029.
[77] M. Rothbauer, J. Strauss, E. I. Reihs, J. Heidenberger, J. Alphonsus, S. Gowers, Y.-C. Chen, J. McLeod, S. Toegel, P. Ertl, R. Windhager, M. Boutelle, D. O'Hare, *Sensors Actuators B Chem* **2025**, *427*, 137123.
[78] D. Bavli, S. Prill, E. Ezra, G. Levy, M. Cohen, M. Vinken, J. Vanfleteren, M. Jaeger, Y. Nahmias, *Natl. Acad. Sci. USA* **2016**, *113*, E2231.
[79] G. Liu, C. Cao, S. Ni, S. Feng, H. Wei, *Microsystems Nanoeng.* **2019**, *5*, 35.
[80] L. J. G. Ouedraogo, M. Kling, N. N. Hashemi, *APL Mater.* **2025**, *13*, 021113.
[81] L. Giampetruzzi, L. Blasi, A. Barca, E. Sciurti, T. Verri, F. Casino, P. Siciliano, L. Francioso, *Bio-Sensing Res* **2022**, *37*, 100512.
[82] M. Odijk, A. D. van der Meer, D. Levner, H. J. Kim, M. W. van der Helm, L. I. Segerink, J.-P. Frimat, G. A. Hamilton, D. E. Ingber, A. van den Berg, *Lab Chip 15*, 745.
[83] J. Yeste, X. Illa, M. Alvarez, R. Villa, *J. Biol. Eng.* **2018**, *12*, 18.
[84] L. Wang, J. Han, W. Su, A. Li, W. Zhang, H. Li, H. Hu, W. Song, C. Xu, J. Chen, *Microsystems Nanoeng.* **2023**, *9*, 2.
[85] P. Schuller, M. Rothbauer, S. R. A. Kratz, G. Höll, P. Taus, M. Schinnerl, J. Genser, N. Bastus, O. H. Moriones, V. Puntes, B. Huppertz, M. Siwetz, H. Wanzenböck, P. Ertl, *Sensors Actuators B Chem* **2020**, *312*, 127946.
[86] J. R. K. Marland, M. E. Gray, C. Dunare, E. O. Blair, A. Tsiamis, P. Sullivan, E. González-Fernández, S. N. Greenhalgh, R. Gregson, R. E. Clutton, M. M. Parys, A. Dyson, M. Singer, I. H. Kunkler, M. A. Potter, S. Mitra, J. G. Terry, S. Smith, A. R. Mount, I. Underwood, A. J. Walton, D. J. Argyle, A. F. Murray, *Bio-Sensing Res.* **2020**, *30*, 100375.
[87] M. Xiao, L. Zheng, X. Zhang, X. Duan, T. Hang, S. Lu, S. Liu, H. Lin, *Anal. Chem.* **2022**, *94*, 748.
[88] J. Gao, J. Carlier, S. Wang, P. Campistron, D. Callens, S. Guo, X. Zhao, B. Nongaillard, *Sensors Actuators B Chem* **2013**, *177*, 753.
[89] M. Sakamiya, Y. Fang, X. Mo, J. Shen, T. Zhang, *Med. Eng. Phys.* **2020**, *75*, 36.
[90] S. O. Catarino, L. R. Silva, P. M. Mendes, J. M. Miranda, S. Lanceros-Mendez, G. Minas, *Sensors Actuators B Chem* **2014**, *205*, 206.

[91] J. U. Lind, T. A. Busbee, A. D. Valentine, F. S. Pasqualini, H. Yuan, M. Yadid, S. J. Park, A. Kotikian, A. P. Nesmith, P. H. Campbell, J. J. Vlassak, J. A. Lewis, K. K. Parker, *Nat. Mater.* **2017**, *16*, 303.
[92] W. Zhao, H. Wang, Y. Guo, K. Sun, Z. Cheng, H. Chen, *Microfluid. Nanofluidics* **2020**, *24*, 88.
[93] R. K. Jayne, M. Ç. Karakan, K. Zhang, N. Pierce, C. Michas, D. J. Bishop, C. S. Chen, K. L. Ekinci, A. E. White, *Lab Chip* **2021**, *21*, 1724.
[94] H. Liu, L. A. MacQueen, J. F. Usprech, H. Maleki, K. L. Sider, M. G. Doyle, Y. Sun, C. A. Simmons, *Biomaterials* **2018**, *172*, 30.
[95] Y. Chen, H. N. Chan, S. A. Michael, Y. Shen, Y. Chen, Q. Tian, L. Huang, H. Wu, *Lab Chip* **2017**, *17*, 653.
[96] J. L. Arlett, E. B. Myers, M. L. Roukes, *Nat. Nanotechnol.* **2011**, *6*, 203.
[97] Q. Wu, J. Liu, X. Wang, L. Feng, J. Wu, X. Zhu, W. Wen, X. Gong, *Biomed. Eng.* **2020**, *19*, 9.
[98] T. Schössler, F. Schön, C. Lemier, G. Urban, *Thin Solid Films* **2020**, *698*, 137877.
[99] D. Resnik, D. Vrtačnik, U. Aljančič, M. Možek, B. Pečar, S. Penič, S. Amon, in IECON Proc. (Industrial Electron. Conf.), IEEE, New York NY USA **2009**, 4014.
[100] G. M. Ferreira, F. M. Azevedo, P. J. Sousa, V. C. Pinto, S. O. Catarino, P. C. Sousa, G. Minas, *Sensors Actuators A Phys.* **2023**, *363*, 114699.
[101] G. M. Ferreira, P. J. Sousa, V. C. Pinto, S. O. Catarino, P. C. Sousa, G. Minas, in *2023 IEEE 7th Port. Meet. Bioeng. ENBENG 2023*, IEEE, New York NY USA **2023**, 5.
[102] R. M. da Ponte, N. Gaio, H. van Zeijl, S. Vollebregt, P. Dijkstra, R. Dekker, W. A. Serdijn, V. Giagka, *Sensors Actuators A Phys.* **2021**, *317*, 112439.
[103] I. M. Gonçalves, R. O. Rodrigues, A. S. Moita, T. Hori, H. Kaji, R. A. Lima, G. Minas, *Bioprinting* **2022**, *26*, 00202.
[104] V. Nock, R. J. Blaikie, T. David, *Lab Chip* **2008**, *8*, 1300.
[105] I. Miranda, A. Souza, P. Sousa, J. Ribeiro, E. M. S. Castanheira, R. Lima, G. Minas, *J. Funct. Biomater.* **2021**, *13*, 2.
[106] Y. Sui, C. A. Zorman, *J. Electrochem. Soc.* **2020**, *167*, 037571.
[107] F. Cantoni, G. Werr, L. Barbe, A. M. Porras, M. Tenje, *HardwareX* **2021**, *10*, 00245.
[108] D. Zeniieh, L. Ledernez, G. Urban, *Procedia Eng* **2014**, *87*, 1398.
[109] Z. G. Ling, K. Lian, L. Jian, Improved patterning quality of SU-8 microstructures by optimizing the exposure parametersin, (Ed: F.M. Houlihan) **2000**, 1019.
[110] J. Wang, *Anal. Chim. Acta* **1999**, *399*, 21.
[111] M. A. Butt, *Coatings* **2022**, *12*, 1115.
[112] G. Clavel, E. Rauwel, M.-G. Willinger, N. Pinna, *J. Mater. Chem.* **2009**, *19*, 454.
[113] M. A. Buttkewitz, C. Heuer, J. Bahnemann, *Curr. Opin. Biotechnol.* **2023**, *83*, 102978.
[114] O. Y. F. Henry, R. Villenave, M. J. Cronce, W. D. Leineweber, M. A. Benz, D. E. Ingber, *Lab Chip* **2017**, *17*, 2264.
[115] B. Chen, Z. Feng, F.-Z. Yao, M.-H. Zhang, K. Wang, Y. Wei, W. Gong, J. Rödel, *npj Flex. Electron.* **2025**, *9*, 58.
[116] J.-F. Lei, H. A. Will, *Sensors Actuators A Phys* **1998**, *65*, 187.
[117] Q. Meng, J. Wang, D. Chen, J. Chen, B. Xie, Y. Lu, *Sensors Actuators A Phys.* **2024**, *369*, 115134.
[118] X. Bai, Y. Du, C. Gai, Y. Guo, Y. Liu, Y. Huang, H. Xu, D. Wu, J. Sun, *Sensors Actuators A Phys.* **2022**, *335*, 113356.
[119] F. Li, S. Yan, C. Lei, D. Wang, X. Wei, J. Yu, Y. Li, P. Ji, Q. Tan, T. Liang, *Micromachines* **2025**, *16*, 516.
[120] S. Sakthinathan, G. A. Meenakshi, S. Vinothini, C.-L. Yu, C.-L. Chen, T.-W. Chiu, N. Vittayakorn, *Processes* **2025**, *13*, 587.
[121] B. K. Dejene, *Mater. Today Adv* **2025**, *28*, 100629.
[122] S.-H. Huang, K.-S. Huang, Y.-M. Liou, *Nanofluidics* **2017**, *21*, 3.
[123] P. Shah, J. V. Fritz, E. Glaab, M. S. Desai, K. Greenhalgh, A. Frachet, M. Niegowska, M. Estes, C. Jäger, C. Seguin-Devaux, F. Zenhausern, P. Wilmes, *Nat. Commun.* **2016**, *7*, 11535.
[124] A. Asif, K. H. Kim, F. Jabbar, S. Kim, K. H. Choi, *Nanofluidics* **2020**, *24*, 43.
[125] M. A. U, Khalid, K. H. Kim, A. R. Chethikkattuveli Salih, K. Hyun, S. H. Park, B. Kang, A. M. Soomro, M. Ali, Y. Jun, D. Huh, H. Cho, K. H. Choi, *Lab Chip* **2022**, *22*, 1764.
[126] V. F. Curto, B. Marchiori, A. Hama, A.-M. Pappa, M. P. Ferro, M. Braendlein, J. Rivnay, M. Fiocchi, G. G. Malliaras, M. Ramuz, R. M. Owens, *Microsystems Nanoeng.* **2017**, *3*, 17028.
[127] M. G. M. Henriques, R. R. Oliveira, D. S. P. J. Teixeira, M. D. L. R. A. Madeira, D. S. P. C. Saraiva, C. C. A. Calaza, European Patent Office, EP4298201B1.
[128] A. Tajeddin, N. Mustafaoglu, *Micromachines* **2021**, *12*, 1443.
[129] R. Gounella, G. M. Ferreira, M. L. M. Amorim, J. N. Soares, J. P. Carmo, *Electronics* **2024**, *13*, 691.
[130] X. Gao, T. Wang, W. Huang, C. Liu, Z. Zhang, Y. Deng, J. Huang, *Biomicrofluidics* **2025**, *19*, 041503.
[131] G. A. Ramírez-González, C. Consumi-Tubito, E. Vargas-Méndez, C. Centeno-Cerdas, *Polymers* **2025**, *17*, 1263.
[132] Y. Jang, J. Jung, J. Oh, *Micromachines* **2023**, *14*, 1736.
[133] J. An, S. Zhang, J. Wu, H. Chen, G. Xu, Y. Hou, R. Liu, N. Li, W. Cui, X. Li, Y. Du, Q. Gu, *Lab Chip* **2024**, *24*, 1586.
[134] J. Li, J. Chen, H. Bai, H. Wang, S. Hao, Y. Ding, B. Peng, J. Zhang, L. Li, W. Huang, *Research* **2022**, *2022*, 9869518.
[135] Y. Li, K. Sun, Y. Shao, C. Wang, F. Xue, C. Chu, Z. Gu, Z. Chen, J. Bai, *Adv. Healthc. Mater.* **2025**, *14*, 2402611.

Gabriel M. Ferreira completed his master's degree in Physics Engineering in February of 2022 by University of Minho, Portugal. In January of 2023, he started a Ph.D. program in Electronic and Computer Engineering, specialization in Instrumentation and Electronic Microsystems also at university of Minho. His research interests include numerical simulators, microfabrication, and microelectronic systems for biomedical applications.

Patrícia C. Sousa received her Ph.D. in Chemical and Biological Engineering from the University of Porto. She is currently an Application and Systems Integration Engineer at the International Iberian Nanotechnology Laboratory (INL). Her work focuses on advanced microfluidic platforms and organ-on-a-chip systems, with emphasis on integrating micro- and nanosensors for real-time monitoring and precise control. She has extensive expertise in micro- and nanofabrication, particularly in nanoimprint lithography, soft lithography, surface engineering, and the development of functional microstructured devices. Her research interests encompass advanced lab-on-a-chip systems, devicesensor integration, and fabrication strategies for biomedical applications.

Susana O. Catarino (MSc 2009, Ph.D. 2014) is an Assistant Professor at the Department of Industrial Electronics of University of Minho (UMinho), Portugal, in the Instrumentation and Electronic Microsystems disciplinary area, and a researcher at the Electromechanical Microsystems Research Center (CMEMS). She received her master's degree in Biomedical Engineering (specialization in Medical Electronics) in 2009 and, in 2014, she concluded her Ph.D. in Biomedical Engineering (in the disciplinary area of Instrumentation and Electronic Microsystems), both from UMinho. She focuses her research in multiphysics simulation for electronic (bio)microsystems, and development and integration of transducers in microfluidic platforms for biotechnology and biomedical applications.

Graça Minas is an Associate Professor with Habilitation at the Department of Electronics Engineering and a researcher at the MicroElectroMechanical Systems Center (CMEMS-UMinho), both at University of Minho (UMinho), Portugal. She received a Ph.D. in Electronics Engineering in 2004 from UMinho, in the field of Lab-on-a-chip devices, working in cooperation with the Laboratory for Electronic Instrumentation, Delft University of Technology, The Netherlands. Her main research interests are in the areas of biomedical microsystems, specifically advanced lab-on-a-chip and organ-on-a-chip devices, on-chip integration of optics, microelectronic circuits and micro(bio)sensors.